https://doi.org/10.5194/egusphere-2026-7022
Preprint. Discussion started: 20 November 2026
© Author(s) 2026. CC BY 4.0 License.

Visualisation of frequency locking of Pleistocene ice age cycles to orbital forcing using Continuous Wavelet Transforms

Diederik Liebrand[1], David A. Hodell[2], and Charlotte S. Miller[3]

[1]Department of Earth Sciences, University College London, London, UK.
[2]Godwin Laboratory for Palaeoclimate Research, Department of Earth Sciences, University of Cambridge, Cambridge, UK.
[3]School of Chemical, Earth and Environmental Sciences, University of Leicester, Leicester, UK.

Correspondence to: Diederik Liebrand (diederik@palaeoclimate.science)

Abstract. We present figures and videos of frequency locking between climate proxy records and orbital forcing based on the Continuous Wavelet Transform (CWT). For this analysis, we employ the sine-Gaussian ("Morlet") wavelet, chosen to optimise the localisation of variance (spectral power) in the time-frequency domain. We first apply this method to benthic and planktic foraminiferal oxygen-isotope ($\delta^{18}O$) records from Iberian Margin Site U1385 spanning the past 1.43 million years (Myr). By tracking the frequencies exhibiting maximum variance through time, the analysis resolves the broad ~110-thousand-year (kyr) eccentricity band into constituent periodicities centred at 90-105 kyr and 120-135 kyr. These periodicities can, at times, be distinguished from harmonics of obliquity (2 × 41 = 82 kyr; 3 × 41 = 123 kyr) and precession (4 × ~23 = ~92 kyr; 5 × ~23 = ~115 kyr). Consistent with previous studies, the CWT results document a shift in the dominant pacing of glacial-interglacial cycles from the 41-kyr obliquity cycle before ~1.25 Ma to eccentricity-modulated precession with periodicities near ~100 kyr after ~0.65 Ma. This transition, corresponding to the Middle Pleistocene Transition (MPT), was characterised by wandering frequency locking among multiples of the obliquity cycle, culminating in the merger of the 2× and 3× obliquity responses and subsequent locking of the climate system onto the 90-105 kyr eccentricity periodicity. Application of the same approach to reconstructed global mean deep-water temperatures (DWT) and continental ice volume ($\delta^{18}O_{seawater}$) indicates that ice-volume variability at the ~100 kyr periodicity was greatest at ~0.40 Ma, when the 90-105 kyr eccentricity periodicity closely approached the projected 2 × 41 kyr obliquity periodicity. In contrast, deep-water temperatures reached maximum variability at the ~100 kyr periodicity at ~0.20 Ma. Finally, we tentatively identify a transition during the last ~150 kyr of the Late Pleistocene that may mark the onset of a new frequency-locking regime, settling onto a dominant climatic response at 3 × 41 kyr.

1. Introduction

1.1. Scope of this study

We analysed benchmark benthic and planktic $\delta^{18}O$ records from Iberian Margin International Ocean Discovery Program (IODP) Site U1385 (Hodell et al., 2023; Hodell et al., 2026), spanning the past 1.43 million years of the Pleistocene, which includes the MPT (Berends et al., 2021; Herbert, 2023). To visualise the changing relationships between climate variability

https://doi.org/10.5194/egusphere-2026-7022
Preprint. Discussion started: 20 November 2026
© Author(s) 2026. CC BY 4.0 License.

and numerical solutions of Earth's orbital parameters (Laskar et al., 2004), we transform multiple CWTs into video clips that facilitate the examination of frequency locking between these records (see Supplementary Movies S1-S4). By compressing 1.43 million years of climate evolution into a few minutes, these videos make it possible to directly observe how frequency locking develops through time. The visualisations highlight the strength of the CWT in time-frequency localisation (Daubechies, 1990; Grinsted et al., 2004), particularly for tracking the evolution of frequencies associated with maximum variance, represented by spectral power ridges (SPRs) (Mitsui, 2026).

To assess the robustness and reproducibility of the observed frequency-locking behaviour, we additionally present a small library of supplementary figures based on equivalent analyses of published benthic and planktic foraminiferal $\delta^{18}O$ stacks (see Supplementary Figures S1 to S117) (Lisiecki and Raymo, 2005; Huybers, 2007; Lisiecki, 2010; Ahn et al., 2017; Zhou et al., 2026). Finally, to explore the climatic significance of the frequency-locking behaviour documented in the Iberian Margin benthic $\delta^{18}O$ record, we extend the analysis to a recently published reconstruction of global mean benthic $\delta^{18}O$, Mg/Ca-derived deep-water temperature (DWT), and the corresponding $\delta^{18}O_{seawater}$ record (Thomas et al., 2026). These records allow us to evaluate whether the frequency-locking patterns observed in the marine isotope record are also expressed in independently reconstructed changes in deep-ocean temperature and global continental ice volume. Together, they provide a visual framework for investigating the evolution of frequency locking of the climate-ocean-cryosphere system to orbital forcing across the MPT and during the Pleistocene.

1.2. The strengths of wavelet analysis

Time-series analysis techniques are fundamental to the investigation of palaeoclimatic records (e.g. (Lourens and Hilgen, 1997; Torrence and Compo, 1998; Schulz and Mudelsee, 2002; Grinsted et al., 2004; Lenoir and Crucifix, 2018a, 2018b; Liebrand and de Bakker, 2019; Liautaud et al., 2020). In this study, we employ CWT analysis using the sine-Gaussian "Morlet" wavelet (Fig. 1a) (Torrence and Compo, 1998; Grinsted et al., 2004). A principal advantage of the CWT over conventional spectral methods is that it does not require a predefined analysis window for all frequencies. Instead, the effective window length scales automatically with the periodicity under investigation (Fig. 1b) (Daubechies, 1990). This adaptive scaling mitigates the inherent trade-off between temporal and frequency resolution. By attaining the minimum time-frequency uncertainty product, the Morlet wavelet provides optimal localisation of variance (i.e., spectral power, or the second central moment) within the time-frequency domain (Daubechies, 1990; Grinsted et al., 2004). This capability is particularly valuable for the analysis of highly non-stationary signals, such as those produced by most palaeoclimate studies (King, 1996). Furthermore, CWT-based analyses can be evaluated against red-noise backgrounds that account for the tendency of many climate and palaeoclimate records to exhibit greater variance at longer periodicities (Hasselmann, 1976; Huybers and Curry, 2006). This permits an objective comparison and ranking of spectral peaks according to their power across the time-frequency domain. Such a property is especially important when identifying climatic states and transitions characterised by dominant periodicities, such as the transition from the "41 kyr world" to the "100 kyr world".

https://doi.org/10.5194/egusphere-2026-7022
Preprint. Discussion started: 20 November 2026
© Author(s) 2026. CC BY 4.0 License.

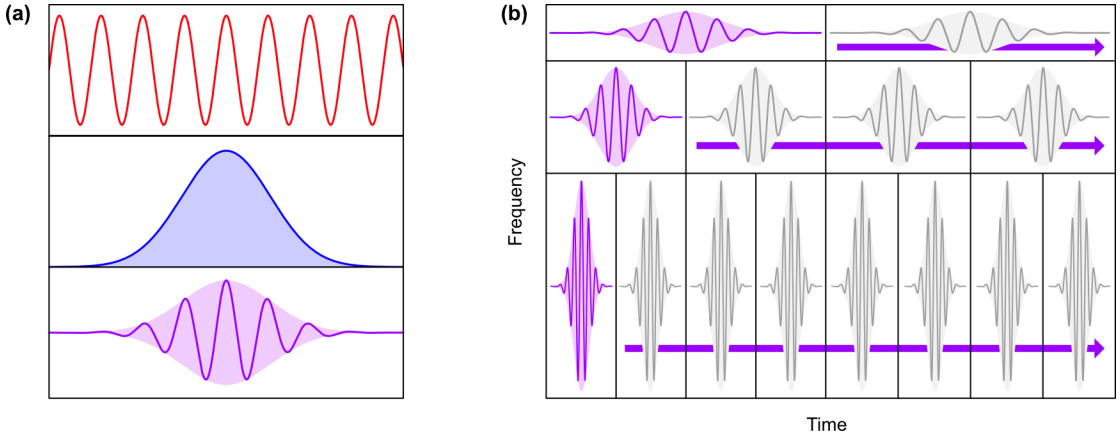
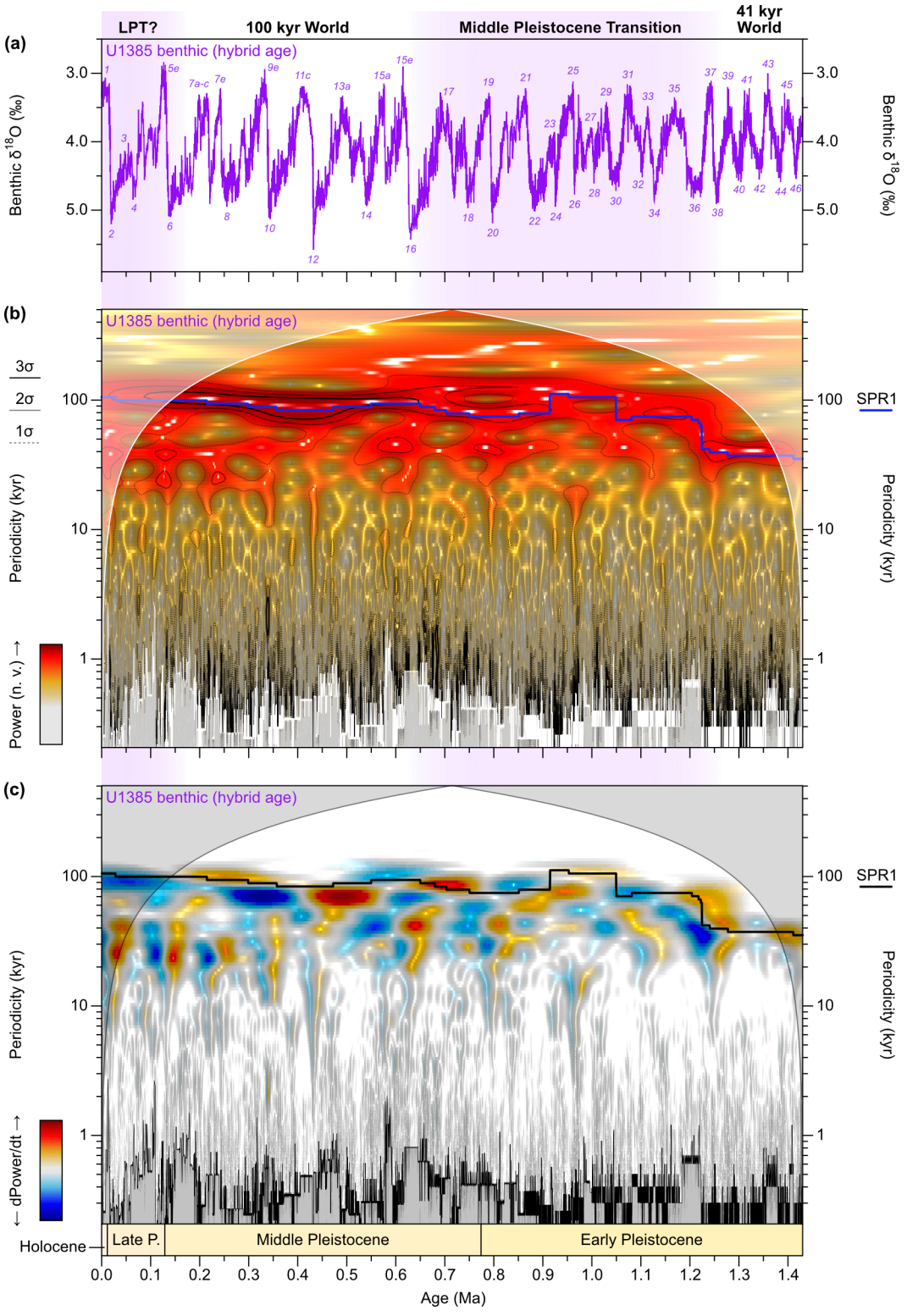


Figure 1: The wavelet analysis optimises time-frequency localisation. (a) The sine-Gaussian Morlet wavelet (purple, bottom), combining a sine wave (red, top) and a Gaussian envelope (blue, middle). (b) Wavelet transform schematic illustrating the adaptive scaling of the analysis window with the periodicity under investigation, where the periodicity-dependent wavelet window-length iteratively slides across the time series (purple arrows) to resolve changes in spectral power through time.

1.3. The Pleistocene from the Iberian Margin

To demonstrate our CWT-movie approach, we apply it to the benthic and planktic foraminiferal $\delta^{18}O$ records from Iberian Margin IODP Site U1385 (Figs. 2 to 7) (Hodell et al., 2023; Hodell et al., 2026). These records span the Early-to-Late Pleistocene (Raffi et al., 2020) from 1.43 to 0.00 Ma. The benthic $\delta^{18}O$ record reflects the combined influence of global continental ice volume and deep-water temperature changes, but the balance between these two controls depends strongly on time scale. On orbital scales (periodicities >10 kyr), benthic $\delta^{18}O$ integrates both ice volume and temperature variability, because global continental ice changes evolve relatively slowly and imprint a longer-periodic signal on $\delta^{18}O_{seawater}$. On millennial scales (periodicities 1–10 kyr), however, ice volume effects become increasingly negligible toward shorter periodicities, and benthic $\delta^{18}O$ variability is dominated by deep-water temperature at 2585 m water depth.

https://doi.org/10.5194/egusphere-2026-7022
Preprint. Discussion started: 20 November 2026
© Author(s) 2026. CC BY 4.0 License.



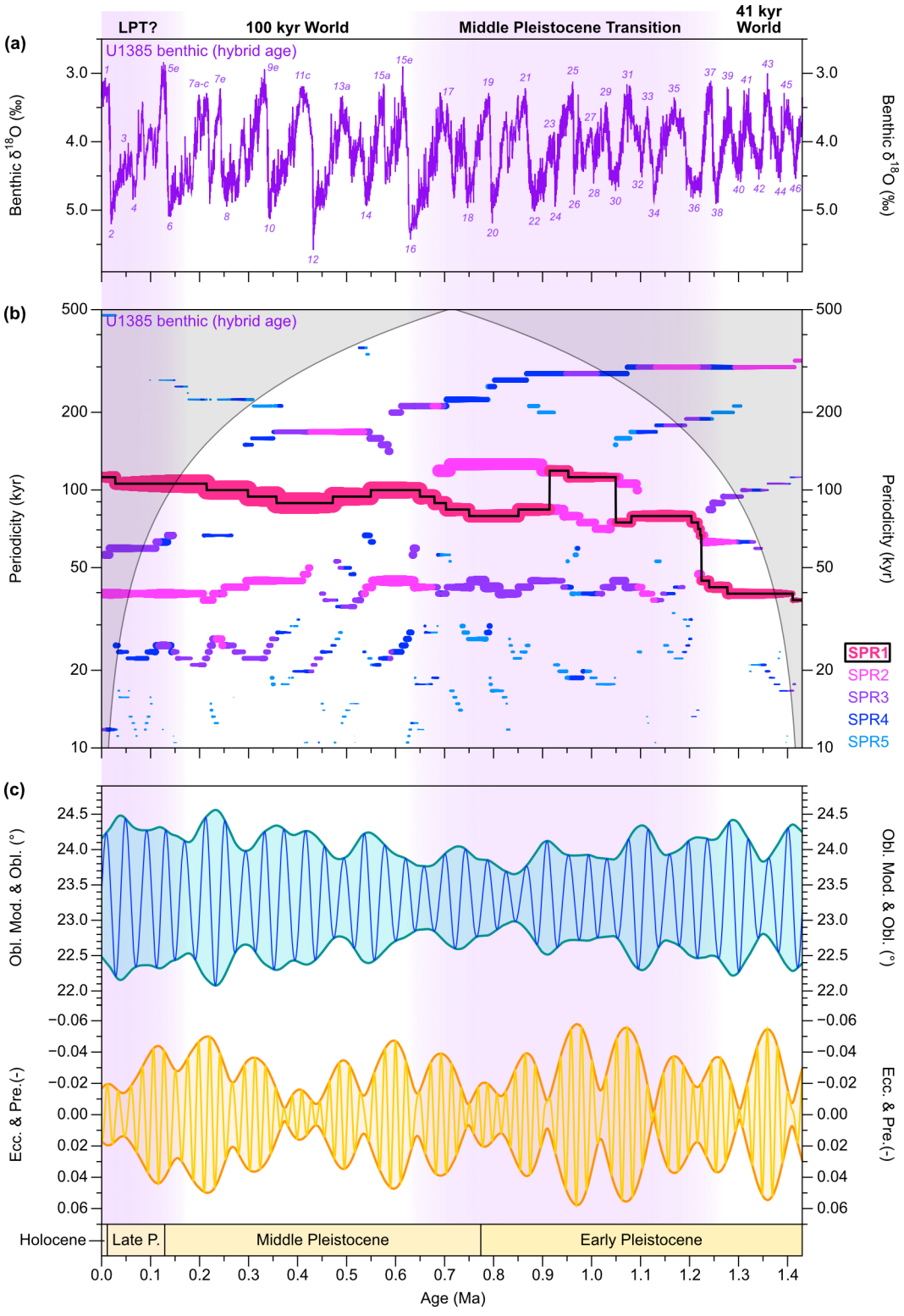
https://doi.org/10.5194/egusphere-2026-7022
Preprint. Discussion started: 20 November 2026
© Author(s) 2026. CC BY 4.0 License.

Figure 2: CWT analysis of the Site U1385 benthic foraminiferal $\delta^{18}O$ record. (a) Site U1385 benthic foraminiferal $\delta^{18}O$ record, based primarily on *Cibicidoides wuellerstorfi* and corrected to *Uvigerina* (Hodell et al., 2023; Hodell et al., 2026). MIS numbers are shown in small purple italics. (b) Standard CWT analysis. Note the emergence of a ~60-kyr periodicity during the last ~150 ka. (c) DCWT analysis highlighting regions of spectral-power gain (orange-red colours) and loss (blue colours) within the time-frequency domain. SPR1 is shown above in blue (panel b) and black (panel c). The COI and regions affected by the Nyquist frequency are shown in semi-transparent white (panel b) and black (panel c). Corresponding analyses of the Site U1385 planktic $\delta^{18}O$ record and additional datasets are provided in the supplementary figures.

As with the benthic record, orbital-scale planktic $\delta^{18}O$ variability arises from a combination of global ice-volume changes and local temperature effects. However, in contrast to the benthic record, planktic $\delta^{18}O$ at Site U1385 records the ambient $\delta^{18}O$ and temperature of subtropical Eastern North Atlantic Central Water, i.e. the surface-to-thermocline water mass in which the planktic foraminifera calcified their tests. On millennial time scales, however, planktic $\delta^{18}O$ is overwhelmingly controlled by temperature variability alone, because surface-water temperatures respond rapidly to North Atlantic climate shifts. This interpretation is supported by the strong correspondence between planktic $\delta^{18}O$ and alkenone-based SST reconstructions from the same site (cf. (Rodrigues et al., 2017; Hodell et al., 2023)), as well as its close similarity to (inverted) Greenland ice $\delta^{18}O$ on both orbital and millennial scales (Shackleton et al., 2000; Hodell et al., 2023).

Together, the benthic and planktic $\delta^{18}O$ records from U1385 illustrate a clear time scale dependence in how foraminiferal $\delta^{18}O$ signals are partitioned between ice-volume and temperature effects. Orbital variability in both records reflects a mixture of the two, whereas millennial variability is dominated by temperature changes; deep-water temperature for the benthic record and surface-water temperature for the planktic record. This dual perspective allows the records from Site U1385 to capture both large-scale Pleistocene ice-volume evolution and the rapid climate oscillations associated with AMOC variability, Dansgaard-Oeschger cycles, and Heinrich events. Also, they provide a unique chronology linking Southern and Northern hemispheric climate-ocean-ice processes (Hodell et al., 2023).

https://doi.org/10.5194/egusphere-2026-7022
Preprint. Discussion started: 20 November 2026
© Author(s) 2026. CC BY 4.0 License.



https://doi.org/10.5194/egusphere-2026-7022
Preprint. Discussion started: 20 November 2026
© Author(s) 2026. CC BY 4.0 License.

Figure 3: Extraction of the first five SPRs from the CWT of the Site U1385 benthic foraminiferal $\delta^{18}O$ record. (a) As in Fig. 2 panel (a). (b) SPR1 to SPR5, colour-coded from cherry pink to light blue, respectively. Line thickness is proportional to spectral power. The black line highlights the evolution of SPR1 through the time-frequency domain. The COI is indicated by the semi-transparent black shading. (c) Orbital solutions for eccentricity, obliquity, and climatic precession (Laskar et al., 2004). Obliquity modulation was calculated using a Hilbert transform. Corresponding analyses of the Site U1385 planktic $\delta^{18}O$ record and additional datasets are provided in the supplementary figures.

1.4. Global mean deep-sea temperature and continental ice volume

Global stacks of benthic $\delta^{18}O$ are often taken as representing global ice volume, but significant temperature effects remain (Shackleton, 2000). The phasing of temperature and ice-volume changes can differ, with temperature leading $\delta^{18}O_{seawater}$ (Elderfield et al., 2012). At ~900 ka during the MPT, $\delta^{18}O_{seawater}$ increased during glacial periods, which has been interpreted as evidence for a substantial expansion of continental ice volume (Elderfield et al., 2012; Ford and Raymo, 2019). Thomas et al. (2026) compiled globally averaged (i.e. basin-volume-weighted) records of benthic Mg/Ca-derived DWT and derived $\delta^{18}O_{seawater}$ documenting basin-scale differences including a cooling of North Atlantic deep waters and increased salinity of the deep Pacific Ocean across the MPT. To further unravel the partitioning of benthic $\delta^{18}O$ into temperature and continental ice-volume (and salinity) contributions, we apply the same CWT analysis to these basin-volume-weighted global stacks of benthic Mg/Ca-derived DWT and corresponding $\delta^{18}O_{seawater}$ (Figs. 8 to 11) (Thomas et al., 2026).

2. Methods

2.1. Earth's astronomical solutions

We analyse the numerical La2004 solutions (Laskar et al., 2004) for orbital eccentricity, obliquity, and climatic precession using the CWT. All three orbital solutions are stable throughout the Pleistocene study interval. Each forcing component is analysed individually because records that combine multiple orbital parameters, such as insolation time series, contain interacting frequencies whose superposition and interference can complicate interpretation and potentially bias the analysis. Climatic precession is conventionally defined such that present-day values are near a maximum, implying that precession minima correspond to maxima in Northern Hemisphere summer insolation. Because Site U1385 is in the Northern Hemisphere, and summer insolation plays a central role in classical Milankovitch Theory, the climatic precession axis is inverted in Figure 3 so that maxima correspond to increased Northern Hemisphere summer insolation.

In addition to the three principal orbital parameters, we consider the amplitude modulation of obliquity. The obliquity modulation shown in Figure 3 was derived from the obliquity solution using the Hilbert transform. Like eccentricity modulation of precession, obliquity exhibits modulation on longer timescales, causing the amplitude of the 41 kyr cycle to vary at higher periodicities, including components near 100 and 180 kyr (Laskar et al., 2004). This modulation is thus of interest because it may introduce power at periodicities comparable to those associated with Pleistocene glacial cycles (Blackburn et al., 2024).

https://doi.org/10.5194/egusphere-2026-7022
Preprint. Discussion started: 20 November 2026
© Author(s) 2026. CC BY 4.0 License.

150

2.2. Climate proxy records

The Site U1385 benthic foraminiferal $\delta^{18}O$ record was generated using a mix of species, mainly *Cibicidoides wuellerstorfi*, and isotopic values were corrected to *Uvigerina* (Hodell et al., 2023). The Site U1385 planktic foraminiferal $\delta^{18}O$ record was produced solely using tests of *Globigerina bulloides*, a surface-ocean mixed-layer dwelling species. The interval spanning
155 Marine Isotope Stage (MIS) 11c/Termination V is affected by a short (~30 kyr) hiatus (Hodell et al., 2023), which was subsequently recovered by redrilling Site U1385 during Expedition 397 (Hodell et al., 2026).

We use the hybrid age model of Hodell et al. (2015), which is based on correlation to Antarctic ice-core records for the past 194 kyr and alignment of sediment colour (L*) to climatic precession for the remainder of the record. This chronology leaves
160 the isotope records largely, though not completely, independent of tuning assumptions (Hodell et al., 2023), insofar as the $\delta^{18}O$ record was not directly tuned to an orbital target. Therefore, especially the response of the climate-cryosphere system to the longer-period orbital components of obliquity and eccentricity can be considered comparatively free from age-model tuning assumptions.

165 To assess the robustness of the results, we additionally analyse several independently tuned and untuned benthic and planktic $\delta^{18}O$ compilations. Tuned and minimally tuned records include LR04 (Lisiecki and Raymo, 2005), Probstack and Probstack LR04 (Ahn et al., 2017), and Bigstack auto, Bigstack mixed, Bigstack mixed Atlantic, and Bigstack mixed Pacific (Zhou et al., 2026). Untuned chronologies include H07 benthic untuned and H07 planktic untuned (Huybers, 2007), LR04 untuned (Lisiecki, 2010), and Bigstack magrev (Zhou et al., 2026). We also analyse recently published globally averaged, basin-
170 volume-weighted records of DWT and $\delta^{18}O_{seawater}$ (Thomas et al., 2026). These records use chronologies aligned to the LR04 benthic $\delta^{18}O$ stack (Lisiecki and Raymo, 2005).

2.3. The continuous wavelet transform

Our supplementary movies are based on the standard CWT using the sine-Gaussian "Morlet" wavelet. Most figures (Figs. 2
175 to 11) and all supplementary figures (Supp. Figs. S1 to S117) are based on subsequent computations derived from the CWT output. All CWTs were computed using the Matlab package of Grinsted et al. (2004), which incorporates code developed by Torrence and Compo (1998).

The numerical solutions of orbital eccentricity, obliquity, and climatic precession were exported at 100-year, 1-kyr, and 3-
180 kyr resolution to match the temporal resolution of the proxy datasets. These time series, as well as the extracted obliquity amplitude modulation, were normalised, but not linearly detrended, prior to analysis. To effectively eliminate edge effects, an additional 1 Myr of data was appended on either side of each astronomical solution before computing the CWT.

https://doi.org/10.5194/egusphere-2026-7022
Preprint. Discussion started: 20 November 2026
© Author(s) 2026. CC BY 4.0 License.

For the supplementary movies (Supp. Movies S1 to S4) and associated figures (Supp. Figs. S1 to S19), the Site U1385 records were linearly detrended, resampled at 100-year resolution, and subsequently normalised prior to CWT analysis. No periodic components were removed. Although some intervals are less highly resolved than others, this approach provides a consistent temporal spacing throughout the record.

For sensitivity and reproducibility tests, the independently tuned and untuned benthic and planktic $\delta^{18}O$ compilations were linearly detrended, resampled at 1-kyr resolution, and normalised prior to analysis (Supp. Figs. S20-S93). To assess the effects of sampling density, the Site U1385 analyses were repeated using both 100-year and 1-kyr resampling intervals (cf. Supp. Figs S9 to S19 to Supp. Figs. S83 to S93, see also Figs. 2 to 7). The globally averaged DWT and $\delta^{18}O_{seawater}$ records were analysed at their published 3-kyr resolution (Figs. 8-10; Supp. Figs. S94-S117).

Where possible, CWTs were computed up to 2.43 Ma, extending 1 Myr beyond the oldest Site U1385 data point to reduce edge effects. Results are only shown for the interval 1.43-0.00 Ma that overlaps with Site U1385. Analyses focus on periodicities up to 500 kyr, corresponding to the maximum periodicity examined in the Site U1385 records. Nyquist frequencies were calculated and displayed where appropriate. CWT results that fall beneath the cone of influence (COI) are less certain and may be affected by edge effects. Wavelet power is expressed as normalised variance (Grinsted et al., 2004). Although the CWT output is calculated on a base-2 logarithmic frequency axis, all figures and movies are displayed on a base-10 logarithmic scale.

2.4. Spectral power ridges

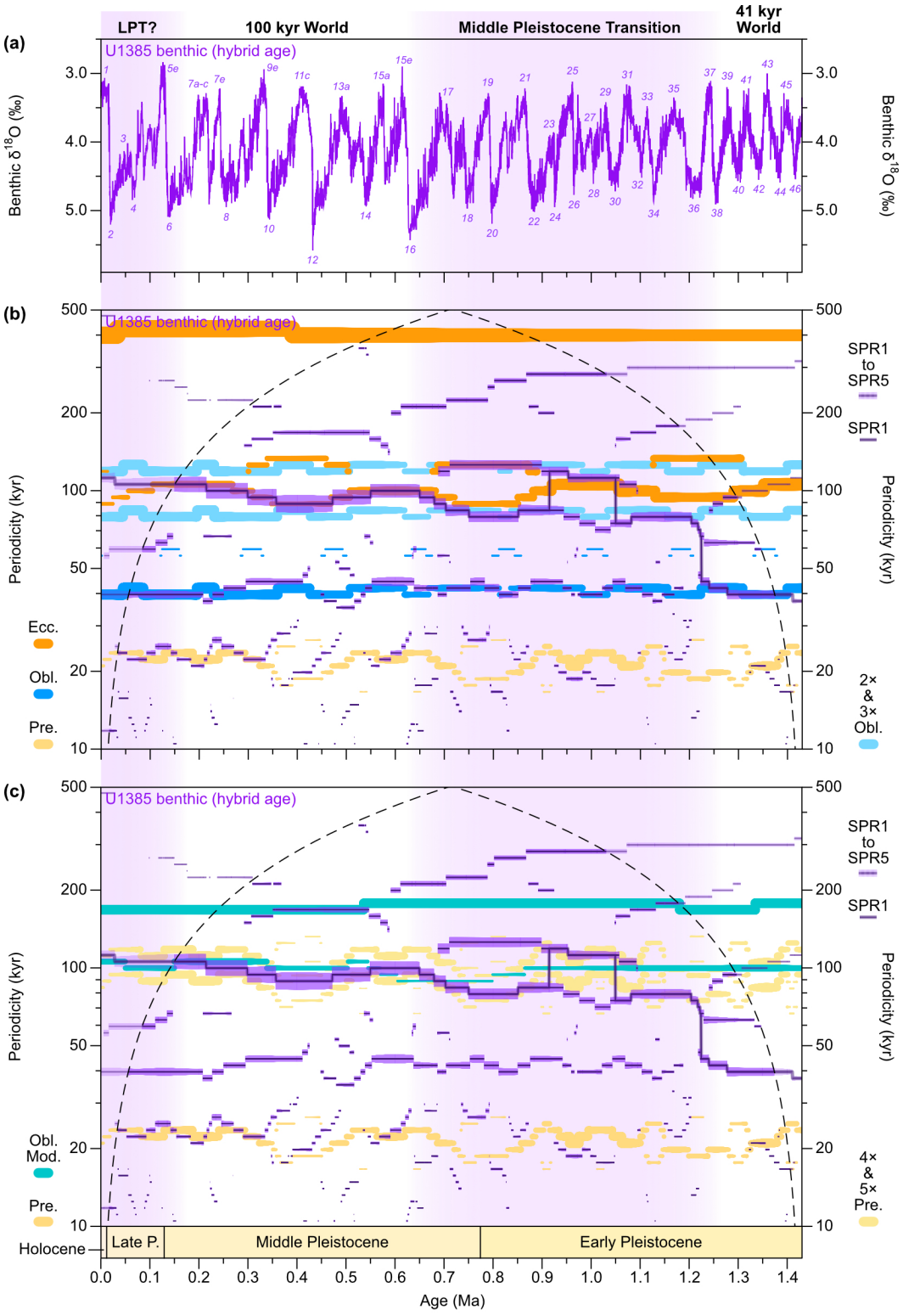
Following CWT analysis of the astronomical solutions and proxy records, SPRs were extracted for the principal orbital periodicities. An SPR represents the continuous path of maximum wavelet power through the time-frequency domain and therefore depicts how the dominant frequency of a signal evolves through time (Mitsui, 2026). SPRs were identified across the full range of periodicities analysed and ranked from 1 to 5 according to decreasing power.

In addition, we computed projected SPRs associated with multiples of the primary 41 kyr obliquity periodicity (38-42 kyr) and the ~23 kyr precession periodicities (16-26 kyr) to assess possible harmonic responses. These projected SPRs are shown as shaded bands in the figures, supplementary figures, and supplementary movies and, where applicable, are assigned the same spectral power as their corresponding SPR1s. We do not compute projected SPRs arising from combination tones, that is, more complex nonlinear responses generated by interactions among the principal orbital frequencies (Liebrand and de Bakker, 2019), and therefore restrict our reassessment of orbital-pacing theory to the simplest forms of nonlinear response, namely the skipping of one or more precession and/or obliquity cycles.

https://doi.org/10.5194/egusphere-2026-7022
Preprint. Discussion started: 20 November 2026
© Author(s) 2026. CC BY 4.0 License.

Comparison of the SPRs derived from proxy records and orbital solutions provides a visual framework for assessing when climatic variability tracks specific orbital periodicities. In most figures, SPR line thickness scales with spectral power. In some cases, however, line thickness is scaled using power and/or log-power, whichever produces the larger visual contrast, for display purposes only; the applied scaling is specified in the figure captions. Where conditional colouring is employed (see Fig. 4, as well as Supp. Figs. S16, and every fifth figure between S30 and S90), colours reflect overlap with orbital SPRs, excluding precession multiples and the ~100 kyr obliquity-amplitude modulation. For the 3 kyr resampled records only (Thomas et al., 2026), the conditional colouring associated with overlap of the projected 3 × 41 kyr obliquity/eccentricity bandwidth (brown colours) was extended by one additional frequency bandwidth to provide a more faithful representation of the underlying pacemaker (Figs. 8 and 9, as well as Supp. Figs. S94, S105, S110, and S115).

https://doi.org/10.5194/egusphere-2026-7022
Preprint. Discussion started: 20 November 2026
© Author(s) 2026. CC BY 4.0 License.



https://doi.org/10.5194/egusphere-2026-7022
Preprint. Discussion started: 20 November 2026
© Author(s) 2026. CC BY 4.0 License.

Figure 4: Comparison of the first five SPRs of the Site U1385 benthic foraminifer $\delta^{18}O$ record with the principal periodicities of the orbital solutions. (a) As in Fig. 2 panel (a). (b) SPR1 to SPR5 (semi-transparent purple colours) compared with eccentricity, obliquity, projected 2 × and 3 × obliquity, and precession (Laskar et al., 2004). These orbital periodicities are included in Supplementary Movies S1 to S3. Width of the proxy SPR lines scales with spectral power. (c) As in panel (b), but compared with obliquity amplitude modulation, precession, and projected 4 × and 5 × precession. The COI in panels (b) and (c) is indicated by a dashed line. The COI applies only to the Site U1385 benthic foraminifer $\delta^{18}O$ record, not to the orbital solutions. Corresponding analyses of the Site U1385 planktic $\delta^{18}O$ record and additional datasets are provided in the supplementary figures.

2.5. CWT Movies

To generate the supplementary movies, we used a MATLAB for-loop routine to iteratively plot and capture multiple CWT spectra at identical time (or frequency) stamps, enabling direct comparison of the spectral evolution of Earth's orbital parameters and climate proxies. SPRs, together with projected 2× and 3× multiples of the 41 kyr obliquity periodicity, are overlain on the CWT spectra. The left y-axis of the movies corresponds to the CWT output of the orbital solutions. Because the CWTs of orbital solutions do not exhibit red-noise behaviour, no red-noise spectra are associated with these panels. The right y-axis corresponds to the CWT output of the proxy records and includes the corresponding red-noise spectra. For Supplementary Movies S3 and S4, the CWT of the planktic foraminiferal $\delta^{18}O$ record was rescaled relative to that of the benthic foraminiferal $\delta^{18}O$ record using their respective red-noise spectra. No equivalent rescaling was applied between the orbital and proxy CWTs because red-noise spectra are not applicable to orbital solutions. Comparisons between orbital and proxy wavelet power should therefore be regarded as qualitative. For Supplementary Movie S4, the frequency axis was interpolated fifty-fold relative to the original 136 frequency bands resolved by the CWT, resulting in a smoother visualisation of spectral evolution (i.e., an appropriate frame rate).

3. Results

3.1. Key to figures, supplementary figures, and supplementary movies

Accompanying this paper are four supplementary movies (Supp. Movies S1 to S4) and a suite of 117 supplementary figures (Supp. Figs. S1-S117). The extensive supplementary figure set provides a comprehensive archive of the CWT analyses underpinning the results presented in the main text. They are included to document the full set of analyses on which our interpretations are based. The first page of each of the three supplementary figures PDF-files provides a key to the figures.

Movie S1 illustrates the CWT spectral evolution of the Site U1385 benthic foraminiferal $\delta^{18}O$ record alongside the astronomical solutions for eccentricity, obliquity, and climatic precession. Movie S2 presents the equivalent comparison for the Site U1385 planktic foraminiferal $\delta^{18}O$ record. Movie S3 combines these analyses, allowing direct comparison of the benthic, planktic, and astronomical CWT spectra within a single animation. Movie S4 presents the same information as Movie S3, but with time plotted on the x-axis rather than periodicity and frequency.

https://doi.org/10.5194/egusphere-2026-7022
Preprint. Discussion started: 20 November 2026
© Author(s) 2026. CC BY 4.0 License.

Figures 2 to 7 highlight selected aspects of the supplementary movies, ranging from changes in wavelet variance between successive movie frames (i.e., difference continuous wavelet transform; DCWT; Fig. 2, panel (c)) to interpretations derived from overlapping SPRs (Figs. 3 to 7). Owing to space limitations, the main text focuses on results from the Site U1385 benthic $\delta^{18}O$ record before examining the globally averaged and basin weighted DWT and $\delta^{18}O_{seawater}$ stacks (Figs. 8 to 11). Results for the Site U1385 planktic $\delta^{18}O$ record, together with the reproducibility tests, are presented in the supplementary figures (Supp. Figs. S14 to S18, and S28 to S92, respectively).

3.2. The Middle Pleistocene Transition according to the CWT

Based on our comprehensive analysis of the Site U1385 records, supported by additional analyses of globally averaged stacks, we identify four key intervals during the MPT in which most records exhibit a shift in the dominant periodicity tracked by their respective SPR1s. These shifts are expressed differently among records, likely reflecting age-model uncertainties and other stack- or record-specific characteristics. Accordingly, the switch points are defined in the frequency domain and should not be interpreted as discrete, synchronous events in the time domain. Instead, they represent broad statistical transitions in the dominant behaviour of the SPR1s, which capture the principal time-frequency localisation of variance within each record. For convenience, we designate these transitions as switch points A to D.

Switch point A (1.30-1.19 Ma; MIS 39-35) marks the termination of the 40 kyr World and, in almost all records except DWT and $\delta^{18}O_{seawater}$, corresponds to a transition towards tracking the projected SPR of a 2 × 41 kyr (~82 kyr) obliquity response. In many records, this transition is progressive rather than abrupt, with tracking of the projected 2 × 41 kyr SPR consolidating over approximately 150-200 kyr.

Switch point B (1.12-1.03 Ma; MIS 33-28) is characterised by an asynchronous response at Site U1385. At 1.11 Ma, the SPR1 of the planktic foraminiferal $\delta^{18}O$ record shifts to a position between (i) the projected SPR of the 3 × 41 kyr (~123 kyr) obliquity response and (ii) the projected SPR associated with the 90-105 kyr eccentricity band. Interpretation is complicated by the fact that this frequency range also overlaps with (iii) the projected SPR associated with a 5 × 16-26 kyr precession response, centred near ~120 kyr. This mixed or ambiguous pacing subsequently characterises the interval between Switch points B and C. At approximately 1.05 Ma, the SPR1 of the Site U1385 benthic foraminiferal $\delta^{18}O$ record converges with that of the planktic record. Most other benthic $\delta^{18}O$ records analysed exhibit a similar transition at roughly the same time.

Switch point B therefore marks the onset of an interval extending to Switch point D during which two dominant periodicities coexist in many proxy records. In several benthic $\delta^{18}O$ records, including Site U1385, SPR1 and SPR2 attain comparable amplitudes during this phase. Switch point B also marks the first instance of $\delta^{18}O_{seawater}$ tracking the projected SPR of the 3 × 41 kyr obliquity response. Towards the end of the interval between Switch points B and C, most records are tracking, or closely approaching, the projected SPR of the 3 × 41 kyr (~123 kyr) obliquity response.

https://doi.org/10.5194/egusphere-2026-7022
Preprint. Discussion started: 20 November 2026
© Author(s) 2026. CC BY 4.0 License.

Switch point C (0.94-0.82 Ma; MIS 24-20) is expressed at Site U1385 as an abrupt and near-synchronous shift of both benthic and planktic $\delta^{18}O$ SPR1s back to tracking the projected SPR of a 2 × 41 kyr (~82 kyr) obliquity response. Simultaneously, their SPR2s migrate in the opposite direction and begin tracking the overlapping projected SPRs associated with the 120-135 kyr eccentricity band and the 3 × 41 kyr (~123 kyr) obliquity response. This structure is broadly reproduced by the other benthic and planktic $\delta^{18}O$ stacks analysed, although the timing of the transition is more variable and generally delayed relative to Site U1385. DWT likewise shifts to tracking a 2 × 41 kyr (~82 kyr) obliquity response. If DWT overtakes ice-volume effects, this may explain the switch observed in the foraminiferal $\delta^{18}O$ records at switch point C. No concurrent change in the SPR1 of $\delta^{18}O_{seawater}$ is recorded.

The interval between switch points C and D is characterised by stable tracking of the projected SPR of a 2 × 41 kyr (~82 kyr) obliquity response by SPR1 in both the benthic and planktic $\delta^{18}O$ records from Site U1385. During this interval, SPR2 tracks the overlapping projected SPRs associated with the 120-135 kyr eccentricity band and the 3 × 41 kyr (~123 kyr) obliquity response.

Switch point D (0.73-0.61 Ma; MIS 17-14) represents the gradual migration of the SPR1s of the Site U1385 benthic and planktic $\delta^{18}O$ records away from the projected SPR of a 2 × 41 kyr (~82 kyr) obliquity response and towards the projected SPR associated with the 90-105 kyr eccentricity band. This migration coincides with a similar migration in the projected SPR associated with a 4 × ~23 kyr (~92 kyr) precession response. During switch point D, SPR1 and SPR2 in all records analysed converge to form a characteristic wishbone structure and subsequently track the projected SPR associated with the 90-105 kyr eccentricity band. No subsequent high-amplitude secondary mode develops during the remainder of the Pleistocene, indicating that a single dominant periodicity accounts for most of the variance thereafter.

3.3. The 100 kyr World according to the CWT

For the interval between 0.61 and 0.15 Ma, corresponding to the 100 kyr World, the SPR1s of the proxy records closely track the projected SPR associated with the 90-105 kyr periodicity of the eccentricity solution (Mitsui, 2026). Earth's orbital eccentricity solution is characterised by gradual changes in both of its principal short-period components, namely the ~90-105 kyr and ~120-135 kyr periodicities. Notably, the 90-105 kyr component evolves from a periodicity of approximately 105 kyr between 0.65 and 0.50 Ma, to approximately 90 kyr between 0.46 and 0.35 Ma, before returning to approximately 105 kyr between 0.26 and 0.10 Ma. The SPR1s of both the Site U1385 benthic and planktic foraminiferal $\delta^{18}O$ records (as well as most other records analysed), tracks this evolving 90-105 kyr eccentricity pattern remarkably closely, indicative of persistent frequency-locking.

https://doi.org/10.5194/egusphere-2026-7022
Preprint. Discussion started: 20 November 2026
© Author(s) 2026. CC BY 4.0 License.

Moreover, the spectral evolution of the climate-cryosphere system during the 100 kyr World can generally be distinguished from alternative projected response modes. In particular, the observed SPR1 trajectories diverge from those associated with tracking (i) the projected SPRs of the 2 × 41 kyr (~82 kyr) and 3 × 41 kyr (~123 kyr) obliquity responses (Fig. 7), (ii) the projected SPRs associated with 4 × ~23 kyr (~92 kyr) and 5 × ~23 kyr (~115 kyr) precession responses, and (iii) the weak amplitude ~100 kyr periodicity associated with obliquity amplitude modulation.

We note that across the broad interval encompassing and surrounding MIS 11 (~0.4 Ma), the SPR associated with the 90-105 kyr eccentricity band closely approached the projected SPR of the 2 × 41 kyr (~82 kyr) obliquity response. This interval corresponds to the highest spectral powers observed during the Pleistocene in most records. Notable exceptions are the planktic $\delta^{18}O$ records and the DWT record. It also coincides with the emergence of a ~180 kyr periodicity in most proxy CWTs linked to obliquity amplitude modulation.

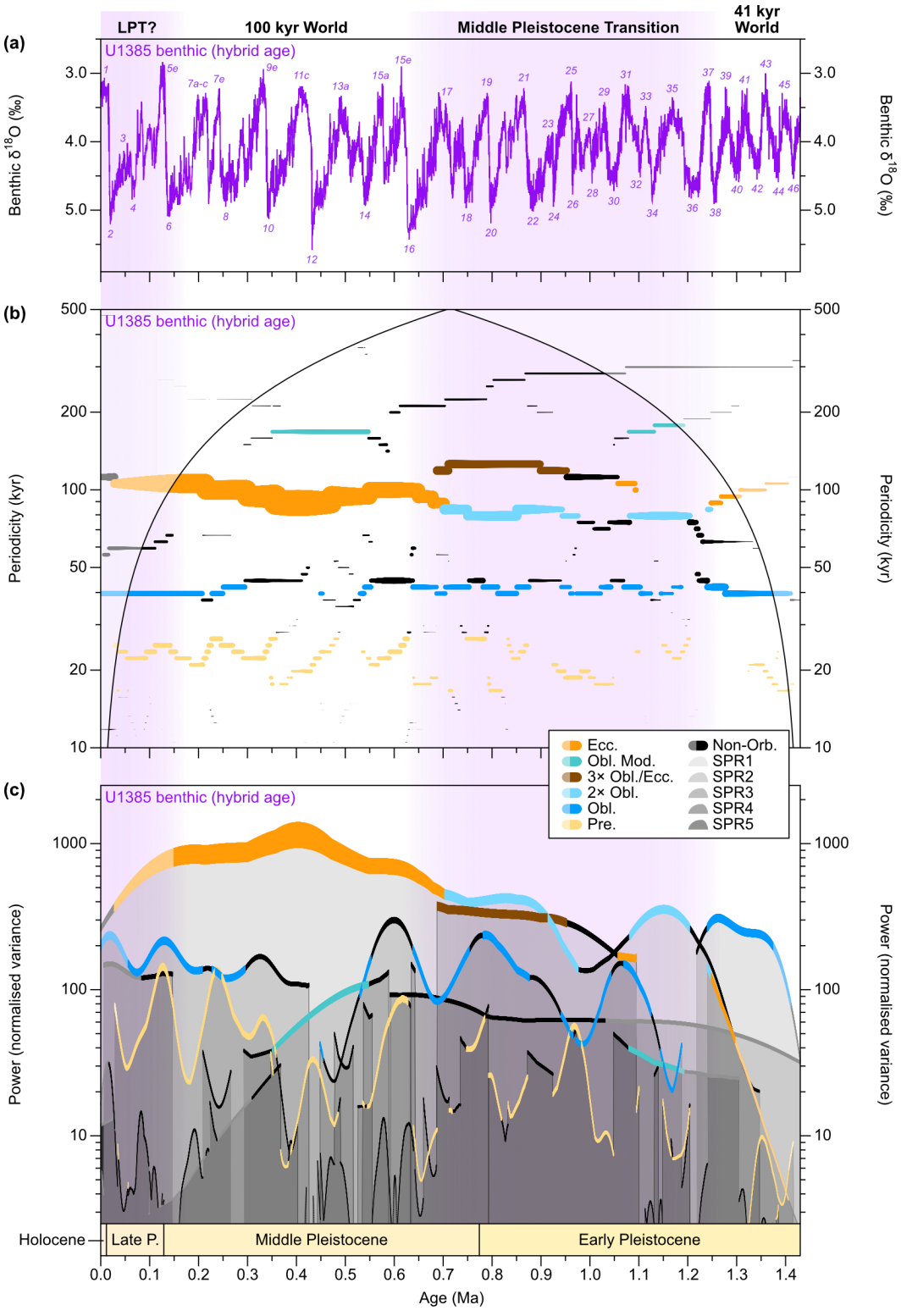
Finally, glacial terminations within the last 0.45 Myr of the 100 kyr World (i.e., especially those post Mid-Brunhes Event) are characterised by offshoot ridges in spectral ridges, particularly in the benthic $\delta^{18}O$ record (Fig. 2), that extend perpendicular to the main ~100 kyr SPR across the spectrum toward precessional frequencies. The DCWT results for the benthic $\delta^{18}O$ records show that peak glacials are associated with increasing power within the obliquity-to-precession frequency range, whereas peak interglacials are characterised by decreasing power within the same range (Fig. 2, Supp. Figs. S83). Some of the largest spectral-power changes identified in the CWT occur at frequencies situated between the principal precession and obliquity bands. Precession steadily intensifies towards the Late Pleistocene, in agreement with other records (e.g., (Liautaud et al., 2020)).

3.4. A potential Late Pleistocene Transition according to the CWT

Based on our analyses, we identify a tentative Late Pleistocene Transition (LPT) extending from approximately 0.15 Ma to the present. We emphasise that the evidence for an LPT remains provisional because the characterisation of dominant periodicities in the continuous wavelet transforms is increasingly affected by edge effects towards the end of the records, resulting in substantial overlap with the cone of influence (COI) (Fig. 7). Consequently, the spectral behaviour described below should be interpreted with caution.

The SPR1s of all records analysed (Fig. 4, and Supp. Figs. S11, S16, etc., to S114) exhibit a near-synchronous departure from their long-standing frequency-locking to the projected SPR of the 3 × 41 kyr (~123 kyr) obliquity response (Fig. 7). An eccentricity-based interpretation is less likely because the SPR associated with the 120-135 kyr eccentricity band, which overlaps with the projected SPR for 3 × obliquity, exhibits very low spectral power throughout the Late Pleistocene (see e.g. Supp. Figs. S2).

https://doi.org/10.5194/egusphere-2026-7022
Preprint. Discussion started: 20 November 2026
© Author(s) 2026. CC BY 4.0 License.



https://doi.org/10.5194/egusphere-2026-7022
Preprint. Discussion started: 20 November 2026
© Author(s) 2026. CC BY 4.0 License.

Figure 5: Conditional colouring of the first five SPRs of the Site U1385 benthic foraminifer $\delta^{18}O$ record (a) As in Fig. 2 panel (a). (b) SPR1 to SPR5, grey shaded and coloured according to their overlap with the main periodicities of eccentricity, obliquity modulation, 3× projected obliquity and/or eccentricity, 2× projected obliquity, obliquity, and precession (Laskar et al., 2004). Non-Orb. stands for non-orbital. The COI is indicated by a semi-transparent white are. (c) As in panel (b) but here for the time-power domain. Thickness of lines scale with power and/or log-power, whichever is greater, for visual effect only. True spectral power can be read off along the y-axis of panel (c). Areas beneath the COI are indicated by shaded colours. Corresponding analyses of the Site U1385 planktic $\delta^{18}O$ record and additional datasets are provided in the supplementary figures.

The LPT, if real, is characterised by a gradual migration of SPR1 across the spectral gap separating the 90-105 kyr and 120-135 kyr eccentricity periodicities. A further characteristic of the proposed LPT is the emergence of a persistent ~60 kyr spectral mode in almost all records analysed. However, except for its initial appearance at approximately 0.15 Ma, this feature also lies almost entirely within the COI and therefore cannot be confidently interpreted as a stable climatic periodicity.

4. Discussion

4.1. Reappraising the pacemakers of the Pleistocene ice ages

Fifty years ago, the identification of precession-, obliquity-, and eccentricity-related spectral peaks in a planktic foraminiferal $\delta^{18}O$ record dated using an age model independent of orbital tuning provided decisive evidence in support of the Milankovitch Theory of the Ice Ages (Hays et al., 1976). Since then, numerous hypotheses and conceptual frameworks have been developed to explain and refine the quasi-periodic structure of Pleistocene climate variability (e.g., (Ridgwell et al., 1999; Raymo and Nisancioglu, 2003; Lisiecki and Raymo, 2005; Maslin and Ridgwell, 2005; Tziperman et al., 2006; Huybers, 2009; Liautaud et al., 2020; Barker et al., 2022; Ganopolski, 2024; Barker et al., 2025), as well as orbital-scale variability in older intervals of Earth history (e.g., (Westerhold et al., 2020)).

Our reassessment does not identify new forcing mechanisms or climate pacemakers. Rather, it re-evaluates previously proposed mechanisms through their expression in the evolving spectral structure of Pleistocene climate records. The results are consistent with nonlinear climate responses to multiples of precession (Ridgwell et al., 1999; Maslin and Ridgwell, 2005), multiples of obliquity (Huybers, 2009; Bajo et al., 2020), the eccentricity modulation of precession (Tziperman et al., 2006), and obliquity amplitude modulation (Blackburn et al., 2024) during different intervals of the Pleistocene. Importantly, many previous studies have focused on the timing of inceptions and terminations in the time domain, threshold behaviour, or other aspects of glacial-cycle dynamics, whereas our analysis directly examines the temporal evolution of spectral variance in the frequency domain.

https://doi.org/10.5194/egusphere-2026-7022
Preprint. Discussion started: 20 November 2026
© Author(s) 2026. CC BY 4.0 License.

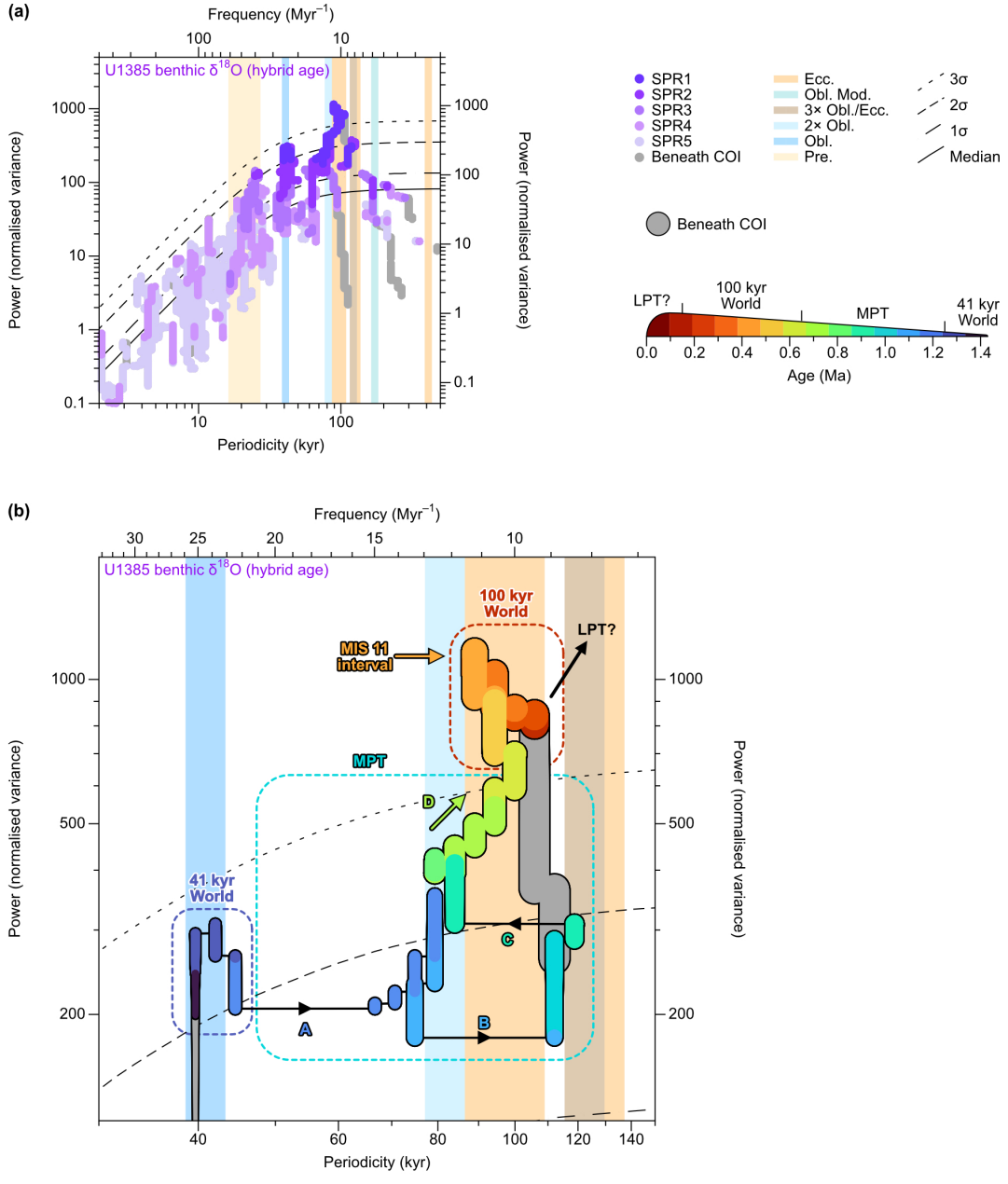


Figure 6: CWT spectra for SPR1 to SPR5. (a) Power spectrum of SPR1 to SPR5 of the Site U1385 benthic foraminifer $\delta^{18}O$ record. (b) Zooming-in on SPR1 from panel (a). MPT switch points, and especially their exact timings, are highly record specific. However, most records follow the A, B, C, D route (see e.g. Supp. Figs. S19, S93, and S117). The broad MIS 11 interval, at ~0.40 Ma, marks the time interval with the highest variance/spectral power concentrated at the 95–105 kyr eccentricity periodicity, which is probably resultant from the close approach to the 2 × 41 kyr (82 kyr) projected obliquity periodicity (i.e., 90-105 kyr eccentricity and 2 × 41 kyr obliquity work together). We speculate on a potential positioning of the LPT in the periodicity-power domain if it had not been affected by the COI. That is, overlapping with the 3 × 41 kyr obliquity harmonic, not the 120-135 kyr eccentricity component, as the latter has very low amplitude in the 100 to 0 ka interval, see e.g. Supp. Fig. S2.).

https://doi.org/10.5194/egusphere-2026-7022
Preprint. Discussion started: 20 November 2026
© Author(s) 2026. CC BY 4.0 License.

410

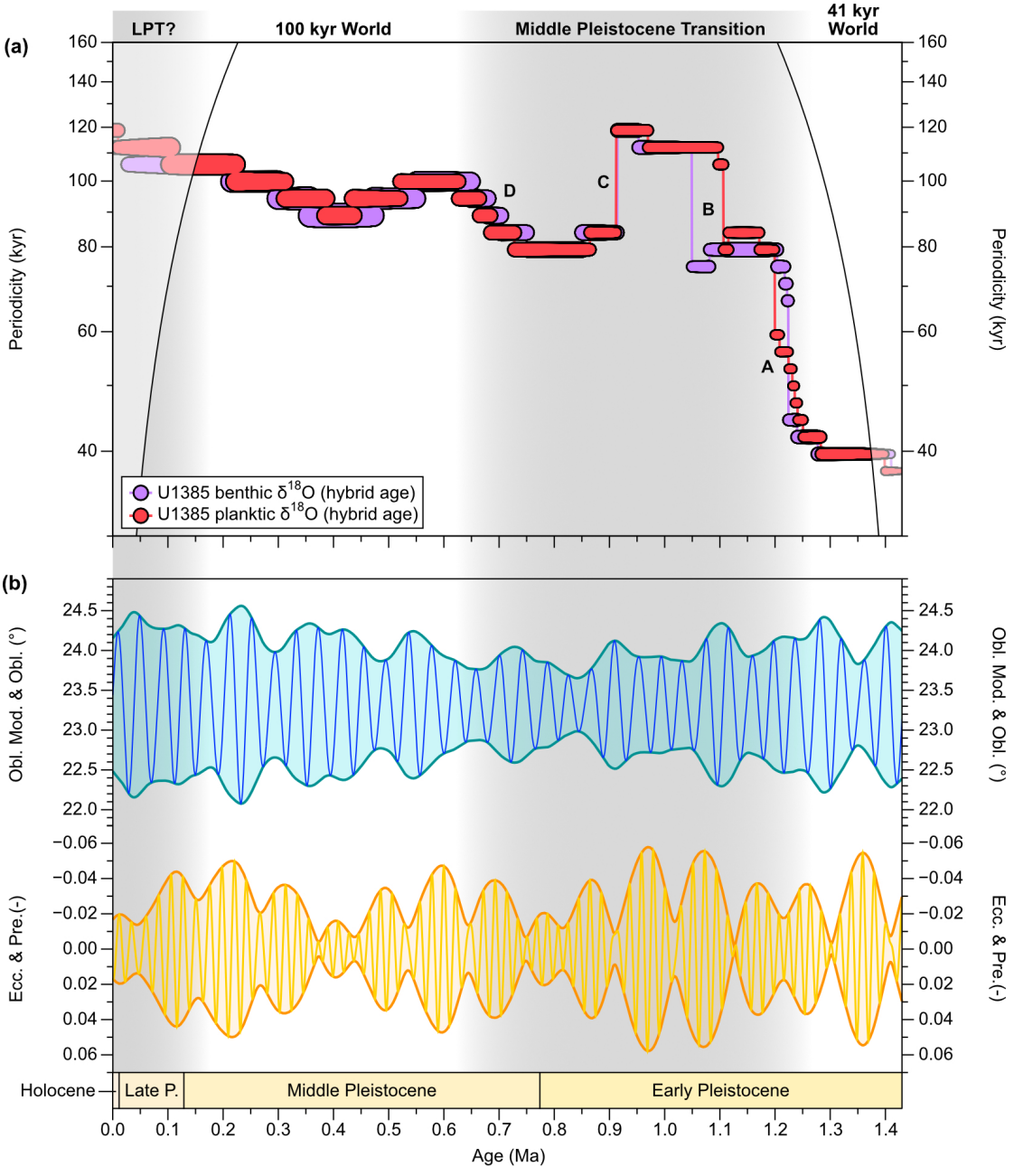


Figure 7: Comparing SPR1s from Site U1385 proxy records. (a) SPR1s of the Site U1385 benthic and planktic $\delta^{18}O$ records. Note the different timings across switch points A and B (see also Supp. Movies S3 and S4 and Supp. Figs. S9 to S19). (b) As in Fig. 3c.

415

https://doi.org/10.5194/egusphere-2026-7022
Preprint. Discussion started: 20 November 2026
© Author(s) 2026. CC BY 4.0 License.

A key advantage of our approach is the use of multiple SPRs, which identify and rank the strongest components of spectral variance in proxy records according to their amplitudes (SPR1-SPR5). The framework also incorporates projected SPRs associated with harmonic responses to obliquity and precession. By tracking changes in the hierarchy of spectral power through time, SPRs provide a concise means of identifying the dominant timescales of climate variability and assessing how their relative importance evolves. Our movies further visualise the evolving spectral landscape and show the complexity and non-stationarity that characterise Pleistocene climate variability.

4.2. The Middle Pleistocene Transition

The change in the dominant amplitude and frequency of the Pleistocene glacial cycles was first noted by Shackleton and Opdyke (1976) who identified a change in the character of the record at ~900 ka (MIS 22) in Core V28-239. Subsequent spectral analysis of the same record by Pisias and Moore (1981) documented the emergence of a pseudo-100-kyr cycle at ~900 ka. At DSDP Site 607, Ruddiman et al. (1989) showed the dominant periodicity of glacial cycles changed from 41-kyr to approximately 100-kyr across the MPT. Whereas the 41-kyrs cycle dominates prior to 1.25 Ma and quasi-100-kyr cycle after 0.65 Ma, the climate response to orbital forcing during the intervening MPT period has been uncertain.

Our analysis of the Site U1385 oxygen isotope records (Figs. 2 to 7, Supp. Figs. S9 to S19, and Supp. Figs. S83 to S92, Supp. Movies S1 to S4) (Hodell et al., 2023; Hodell et al., 2026), supported by repeat analyses of globally averaged stacks (Figs. 8 to 11, Supp. Figs, S28 to S82, and Supp. Figs. S102 to S117) (Lisiecki and Raymo, 2005; Huybers, 2007; Lisiecki, 2010; Ahn et al., 2017; Thomas et al., 2026; Zhou et al., 2026), suggests that the MPT is best viewed as an intermediate state between the 41 kyr World and the 100 kyr World. Switch point A is marked by MIS 35, a notable exception because it reflects a skipped glacial inception rather than a skipped deglaciation. More generally, our CWT analyses show that the MPT was not characterised by an abrupt shift from one dominant periodicity to another. Instead, the climate system exhibited the coexistence of several orbital-scale beats, most notably the ~82 kyr (2 × 41 kyr) and ~123 kyr (3 × 41 kyr) obliquity-derived periodicities. Although these frequencies dominate the spectral structure of the interval, we cannot fully exclude contributions from ~92 kyr and ~115 kyr precession-derived periodicities (4 × and 5 × precession multiples, respectively) to the spectral behaviour of benthic and planktic $\delta^{18}O$ records between switch points B and C and during switch point D. Globally and regionally averaged stacks also exhibit varying alignments with precession- and obliquity-derived periodicities depending on the age model employed. However, analyses of the globally averaged deep-water temperature (DWT) and $\delta^{18}O_{seawater}$ chronologies of Thomas et al. (2026) reveal a more internally consistent evolutionary pattern than is apparent from benthic and planktic isotope records alone (Figs. 8 and 9).

Following switch point B (1.12-1.03 Ma), $\delta^{18}O_{seawater}$ becomes dominated by the ~123 kyr (3 × 41 kyr) obliquity-derived periodicity. This behaviour is consistent with interpretations that the transition from the 41 kyr World to the 100 kyr World reflects evolving North American ice-sheet dynamics (Bintanja and van de Wal, 2008; Abe-Ouchi et al., 2013), whereby

https://doi.org/10.5194/egusphere-2026-7022
Preprint. Discussion started: 20 November 2026
© Author(s) 2026. CC BY 4.0 License.

intrinsic modes of ice-sheet variability increasingly locked onto longer-period obliquity-derived beats that fall within the broad eccentricity frequency band.

During switch point C (0.94-0.82 Ma), DWT becomes dominated by the ~82 kyr (2 × 41 kyr) obliquity-derived periodicity, suggesting that ocean and ice-sheet responses were beginning to converge, albeit not yet onto a common frequency. The emergence of the ~82 kyr beat in DWT may explain the contemporaneous migration of SPR1 in the benthic and planktic $\delta^{18}O$ records from the ~123 kyr (3 × 41 kyr) to the ~82 kyr obliquity-derived periodicity. In this framework, the transition reflects the increasing influence of DWT variability relative to $\delta^{18}O_{seawater}$ within the composite benthic $\delta^{18}O$ signal. This interval partially encompasses the 900-kyr event (MIS 25-21), which has erroneously been described as the first 100-kyr cycle (see discussion in (Bajo et al., 2020)).

By switch point D (0.73-0.61 Ma), the spectral responses recorded in DWT and $\delta^{18}O_{seawater}$ have largely converged, right before substantially larger ice volumes are reconstructed (Thomas et al., 2026). In both records, SPR1 and SPR2 track the same periodicities from switch point C onward, culminating in the emergence of a dominant ~100 kyr beat that characterises the pacing of the Late Pleistocene climate system. The emergence of frequency locking to eccentricity suggests that the intrinsic response time of the global, yet North American-dominated, ice-sheet system became increasingly aligned with the dominant 90-105 kyr eccentricity band as the dominant spectral responses of the ice sheets and deep ocean converged. The spectral evolution implies that this coupled ice sheet-deep ocean system preferentially expressed frequencies near ~100 kyr over neighbouring periodicities near ~82 kyr and ~123 kyr. Because oceans and ice sheets amplify one another through multiple feedbacks, the MPT may reflect the progressive merger of oscillatory modes within previously distinct climate subsystems. In this view, the transition to the 100 kyr World reflects the emergence of a coupled ocean-cryosphere mode, while not precluding an important role for evolving ice-sheet interactions (Bintanja and van de Wal, 2008). Numerous studies have shown that the MPT was marked by major oceanographic reorganisations (e.g. (Petrick et al., 2018; Petrick et al., 2019)). Bispectral analysis has shown that, by switch point D, obliquity overtook precession as the principal source of energy transferred to the eccentricity band through nonlinear frequency coupling (Liebrand and de Bakker, 2019).

Nevertheless, the occurrence of 2 × 41 kyr and 3 × 41 kyr periodicities within $\delta^{18}O_{seawater}$ indicates that these periodicities may, at least in part, originate from global ice volume variability itself, reflecting differences between ice sheets in response times and hysteresis behaviour under orbital forcing (Abe-Ouchi et al., 2013). Bintanja and van de Wal (2008) proposed a related mechanism in which progressive coupling and eventual merger of the Laurentide and Cordilleran ice sheets gave rise to the late-Quaternary 100 kyr cycle. However, $\delta^{18}O_{seawater}$ values during the MPT generally remain below those associated with the largest glaciations of the past ~900 kyr, suggesting that ice volumes may not have been sufficient to facilitate the Laurentide-Cordilleran merger invoked in their model. Moreover, the Cordilleran Ice Sheet may not have contained sufficient ice volume to exert a substantial independent influence on globally integrated $\delta^{18}O_{seawater}$. Although geological

https://doi.org/10.5194/egusphere-2026-7022
Preprint. Discussion started: 20 November 2026
© Author(s) 2026. CC BY 4.0 License.

evidence capable of directly testing such a merger hypothesis is absent, repeated expansions of the Laurentide and Cordilleran ice sheets during subsequent glacial cycles would have extensively eroded and overprinted older glacial landscapes, making it unlikely that geomorphological evidence for any MPT-age ice-sheet merger, even if it once existed, could have survived to the present day. Alternatively, the Antarctic Ice Sheet may have transitioned from predominantly terrestrial melting margins to marine-based margins during the MPT (Raymo et al., 2006; Wirths et al., 2025). Because $\delta^{18}O_{seawater}$ reflects the integrated signal of multiple Northern and Southern Hemisphere ice sheets, the spectral evidence alone does not permit causal attribution of the observed periodicities to particular ice sheets. Further modelling studies could help determine the conditions under which individual ice sheets exhibit 2 × 41 kyr and 3 × 41 kyr hysteresis behaviour and associated equilibrium states.

https://doi.org/10.5194/egusphere-2026-7022
Preprint. Discussion started: 20 November 2026
© Author(s) 2026. CC BY 4.0 License.

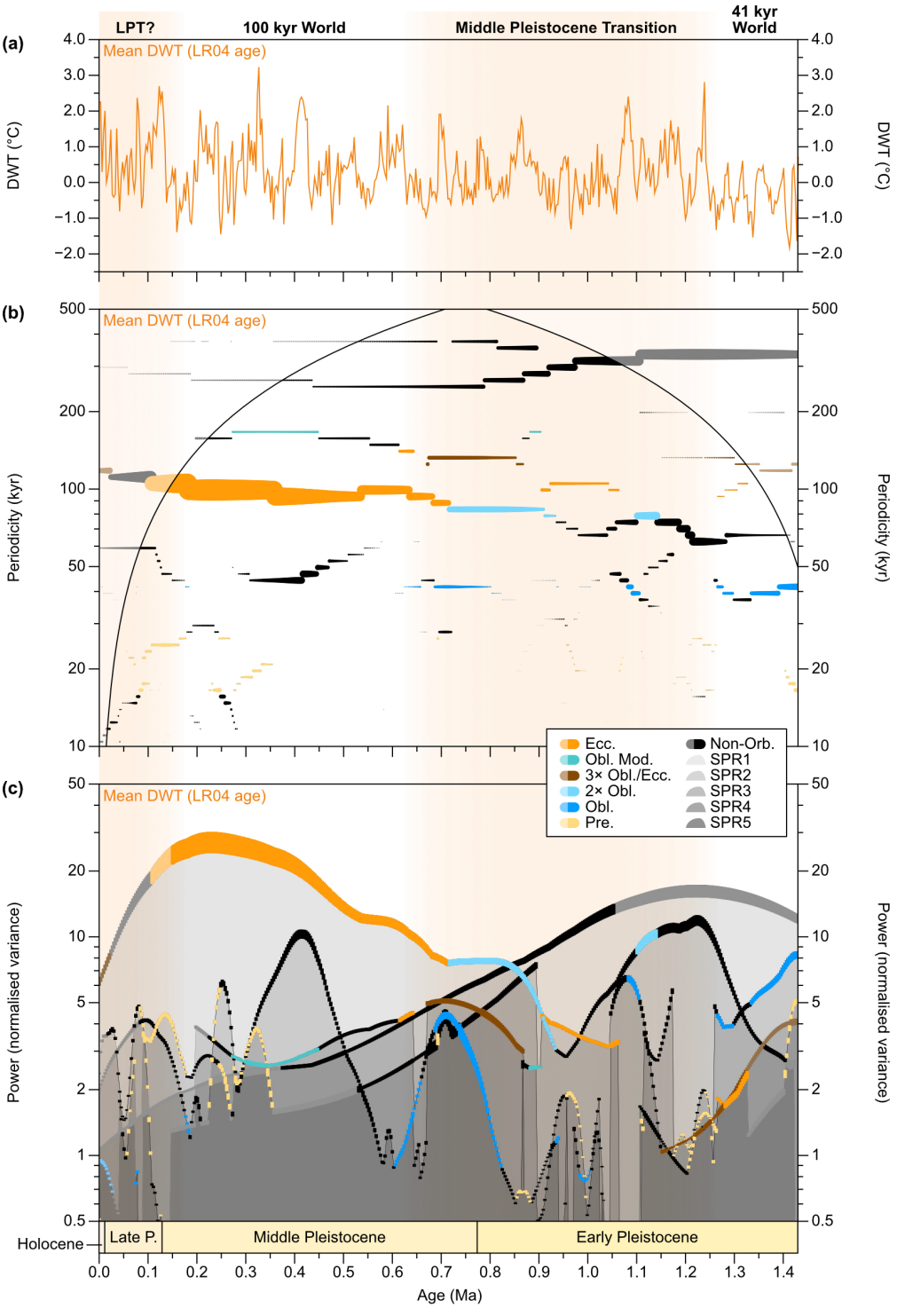


Figure 8: As in Fig. 5, but here for DWT. See Supp. Figs. S107 to S111 for additional CWT analyses on DWT.

https://doi.org/10.5194/egusphere-2026-7022
Preprint. Discussion started: 20 November 2026
© Author(s) 2026. CC BY 4.0 License.

4.3. The 100 kyr World

Our CWT animations further emphasise the distinction between the MPT and the 100 kyr World. One of the two principal eccentricity periodicities, represented by the 90-105 kyr SPR in Fig. 7, evolves from approximately 105 kyr at ~0.60 Ma to ~90 kyr at ~0.40 Ma before returning to ~105 kyr by ~0.20 Ma. This evolution is closely mirrored by the dominant SPRs in both benthic and planktic foraminiferal $\delta^{18}O$ records, indicating a persistent coupling between climate variability and the evolving structure of eccentricity-band periodicities. This correspondence was recently identified independently by Mitsui (2026). The onset of the 100 kyr World at ~0.65 Ma coincides with the appearance of the first oversized Northern Hemisphere ice sheets, as reflected by the occurrence of the first Heinrich event (Hodell et al., 2008).

Attention is drawn to the interval centred on MIS 11, broadly spanning MIS 13a to MIS 10 (ca. 0.40 Ma), which is prominent in most of our CWT analyses, with the notable exceptions of the Site U1385 planktic $\delta^{18}O$ and DWT records. We propose that the exceptional variance in the 100 kyr band during this interval can be explained by the near convergence of the projected SPR associated with the ~82 kyr (2 × 41 kyr) obliquity-derived periodicity and the SPR associated with the 90-105 kyr eccentricity band, the latter being closely tracked by the proxy records. During MIS 11, these periodicities become nearly indistinguishable, potentially allowing their influences to reinforce one another. The benthic $\delta^{18}O$ record exhibits a particularly strong response during this interval, a feature that is also reproduced in all other benthic stacks. Significantly, MIS 11 was the first post-Mid Brunhes Event interglacial characterised by both high atmospheric CO_2 concentrations and pronounced warmth (Bereiter et al., 2015), suggesting that interactions between the climate and carbon cycles may have amplified the response on eccentricity-band timescales in conjunction with constructive interference with the 2 × 41 kyr obliquity periodicity.

https://doi.org/10.5194/egusphere-2026-7022
Preprint. Discussion started: 20 November 2026
© Author(s) 2026. CC BY 4.0 License.

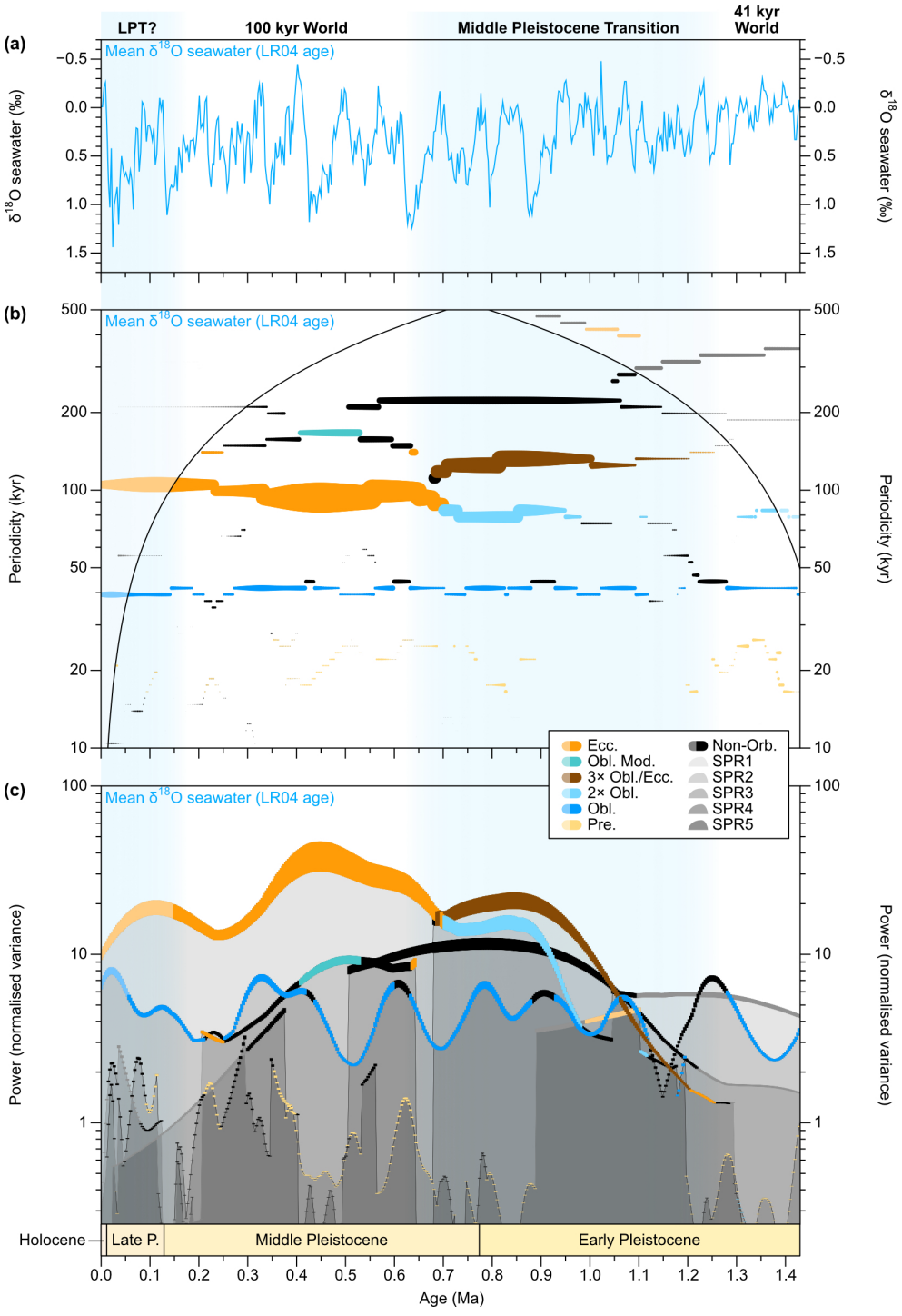


Figure 9: As in Fig. 5, but here for $\delta^{18}O_{seawater}$. See Supp. Figs. S112 to S116 for additional CWT analyses on $\delta^{18}O_{seawater}$.

https://doi.org/10.5194/egusphere-2026-7022
Preprint. Discussion started: 20 November 2026
© Author(s) 2026. CC BY 4.0 License.

4.4. Toward a full bipolar icehouse state?

Here, we explore evidence for a potential LPT, which may represent a previously unrecognised departure of the global climate-cryosphere system from the 100 kyr World (Figs. 3, 4, 7-11; Supplementary Movies S1-S3). We acknowledge that the apparent transition may reflect a statistical artefact rather than a genuine climatic phenomenon. Consequently, the evidence presented here should be regarded as provisional.

Nevertheless, several observations suggest that the LPT warrants further consideration. Between ~0.10 and 0.00 Ma, the shorter of the two principal ~110 kyr eccentricity periodicities migrates from approximately 105 kyr to 90 kyr (Fig. 7). Despite this evolution in the orbital solution, none of our analysed records exhibit a corresponding SPR1 migration toward 90 kyr. Instead, almost all records evolve toward periodicities centred near ~120 kyr, consistent with the ~123 kyr (3×41 kyr) obliquity-derived periodicity (eccentricity has low amplitude at 120-135 kyr periodicity at present). If the climate-cryosphere system had remained fully locked to the evolving 90-105 kyr eccentricity band, a return toward a 90 kyr response would be expected near the present, which would make the last glacial cycle more comparable to the broad MIS 11 interval. Such behaviour is not observed. We have tested for such a migration using a clipped eccentricity solution (0-1.43 Ma, not shown), which is similarly affected by the COI, also showing a migration to the 120-135 kyr periodicity. This would lend further support to the fact that the LPT is indeed a statistical artifact. However, age control for the most recent glacial cycle is exceptionally robust. Independent chronologies, including U-Th constraints spanning the interval between Terminations II and I, indicate a duration of approximately 120 kyr between the onset of the Eemian and the onset of the Holocene (Cheng et al., 2009). Although termination spacing is not identical to attributing the most variance to a periodicity in the wavelet, the difference between the observed duration of the last glacial cycle and the contemporaneous ~90 kyr eccentricity periodicity is striking. The most recent glacial cycle may have been up to ~30 kyr longer than expected from CWT analysis of the eccentricity solution. And it may constitute the first instance during the past 1.43 Ma in which the climate system fully traversed the spectral gap separating the dominant 90-105 kyr and 110-125 kyr eccentricity bands.

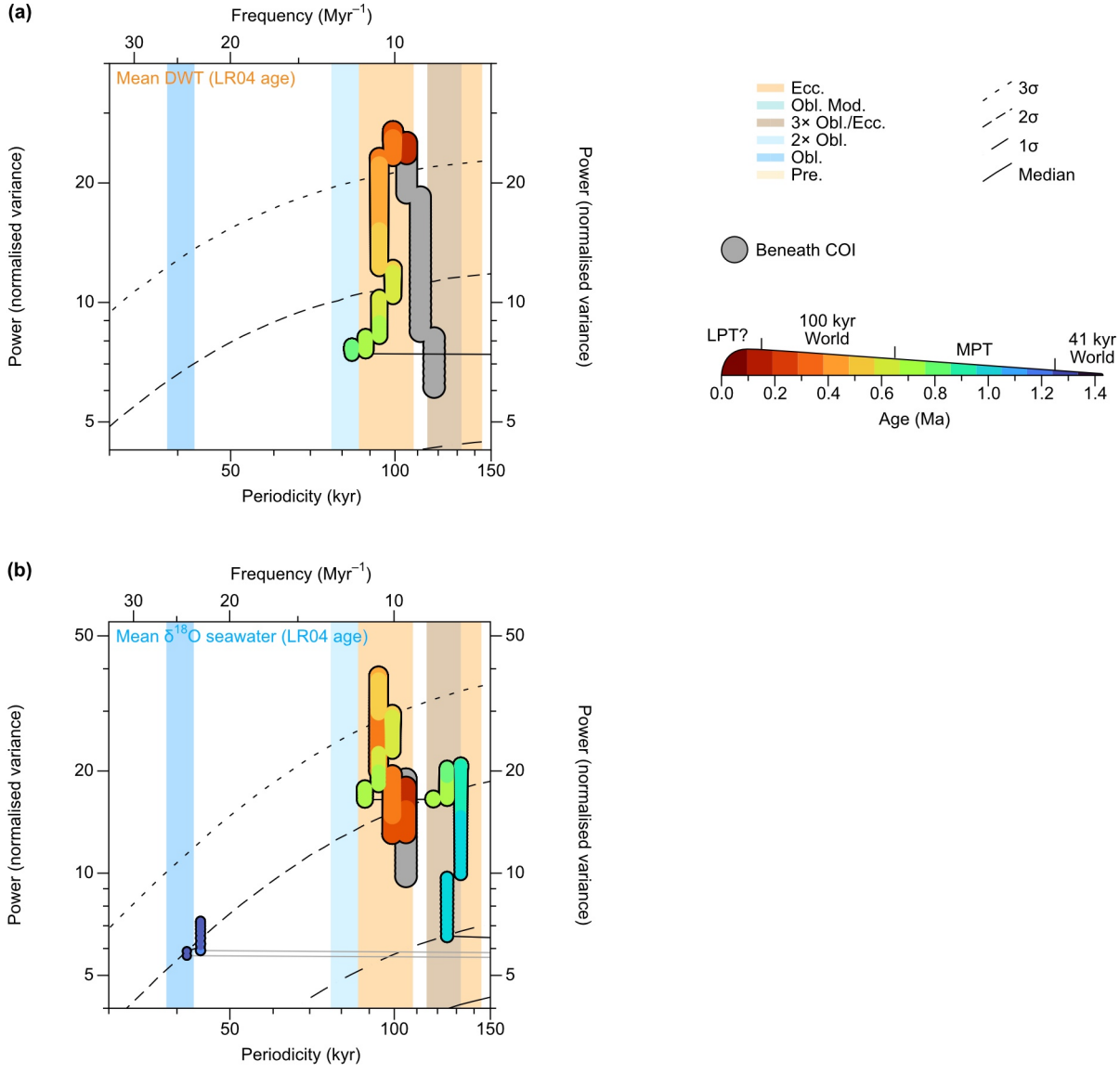
Additional support for a potential LPT comes from the emergence of a ~60 kyr periodicity, observed in almost all record analysed (see supplementary figures). For example, between ~0.13 and 0.00 Ma, a distinct ~60 kyr SPR3 appears in both benthic and planktic $\delta^{18}O$ records (Figs. 2 to 5, Supp. Figs. S9 to S12 and S14 to S17). Although part of this signal lies beneath the COI, its onset occurs outside the zone affected by edge effects, suggesting that it may represent a genuine feature of Late Pleistocene climate variability rather than an artefact of wavelet analysis. We speculate that the 60 kyr cycle may be the first higher harmonic (i.e., 2f) of the 120 kyr periodicity that characterised the last glacial cycle. No ~60 kyr periodicity is observed in the aforementioned CWT analysis of the clipped eccentricity solution, supporting a harmonic interpretation of the 60 kyr cycle as documented in the proxy CWTs.

https://doi.org/10.5194/egusphere-2026-7022
Preprint. Discussion started: 20 November 2026
© Author(s) 2026. CC BY 4.0 License.

One possibility is that the LPT reflects the initial development of a more strongly glaciated, fully bipolar icehouse state (Crowley and Hyde, 2008), consistent with the expectation (outside the COI) that longer periodicities are associated with larger-amplitude glacial-interglacial variability and potentially more extensive glaciation (Fig. 10). Energy-balance modelling suggests that extensive Eurasian mid-latitude glaciation could produce a more hemispherically symmetric icehouse configuration than that observed during most of the Late Pleistocene (Crowley and Hyde, 2008). Within this framework, the apparent departure from the characteristic pacing of the 100 kyr World could signal a gradual reorganisation of the climate-cryosphere system toward such a state. The anomalous millennial scale climate variability of the last glacial cycle (Hodell et al., 2023) may be consistent with this interpretation.

If confirmed, the LPT would constitute a younger boundary of the 100 kyr World. The latter would then represent a transient synchronisation to eccentricity, enabling the climate system to cross the spectral gap between the projected 2× and 3× obliquity periodicities. Such a transient synchronisation with eccentricity would be analogous to those identified for the Antarctic Ice Sheet during the Oligocene and Early Miocene (Liebrand et al., 2017). A notable difference, however, is that the Pleistocene Northern Hemisphere ice sheets were centred on a 400 kyr eccentricity minimum at ~0.4 Ma, whereas the Antarctic synchronisation intervals coincided with 400 kyr eccentricity maxima (Liebrand et al., 2017).

https://doi.org/10.5194/egusphere-2026-7022
Preprint. Discussion started: 20 November 2026
© Author(s) 2026. CC BY 4.0 License.



570 **Figure 10: As in Fig. 6 panel (b), but here for (a) DWT and (b) $\delta^{18}O_{seawater}$. See Supp. Figs. S107 to S116 for additional CWT analyses on $\delta^{18}O_{seawater}$, as well as Supp. Figs. S102 to S106 for the CWT analyses on global mean benthic $\delta^{18}O$.**

4.5. On the absence of a 400 kyr and presence of a 200 kyr periodicity in the Pleistocene

Our CWT analyses of the benthic $\delta^{18}O$, DWT, and $\delta^{18}O_{seawater}$ records further highlight the striking absence of strong 400 kyr
575 eccentricity power in Pleistocene ice-age cycles (de Boer et al., 2014). The 400 kyr periodicity rarely ranks among the five highest-amplitude SPRs (Figs. 9 and 10; Supplementary Movie S4), in marked contrast to many pre-Pleistocene Cenozoic climate and carbon-cycle records (Westerhold et al., 2020). This muted 400 kyr response underscores a fundamental

https://doi.org/10.5194/egusphere-2026-7022
Preprint. Discussion started: 20 November 2026
© Author(s) 2026. CC BY 4.0 License.



difference between Pleistocene climate-carbon cycle variability and the orbital responses that characterised much of the earlier Cenozoic (Kirtland Turner, 2014; Zhang et al., 2025).

One possible explanation is that 400 kyr power was transferred to a 200 kyr periodicity, which is present in some, though not all, of the CWT analyses. Such a higher-harmonic response of the climate-carbon cycle system to 400 kyr eccentricity may have facilitated a redistribution of power from the 400 kyr band to the 200 kyr band, potentially helping to explain the muted Pleistocene expression of the 400 kyr cycle (de Boer et al., 2014). Alternative explanations for the 200-kyr periodicity, although less likely, include a strong nonlinear response, via precession-amplitude modulation, to the weak ~200 kyr component present in eccentricity solutions (see, e.g., Supplementary Movies S1-S3 and Supplementary Fig. S2), or a lower-harmonic response to one or more of the ~110 kyr periodicities. Future work may help discriminate among these possibilities. Pending a robust discrimination between orbital and non-orbital origins, we conservatively classify the 200-kyr periodicity as non-orbital and therefore do not depict a projected ½ × 400 kyr eccentricity SPR for this periodicity.

https://doi.org/10.5194/egusphere-2026-7022
Preprint. Discussion started: 20 November 2026
© Author(s) 2026. CC BY 4.0 License.

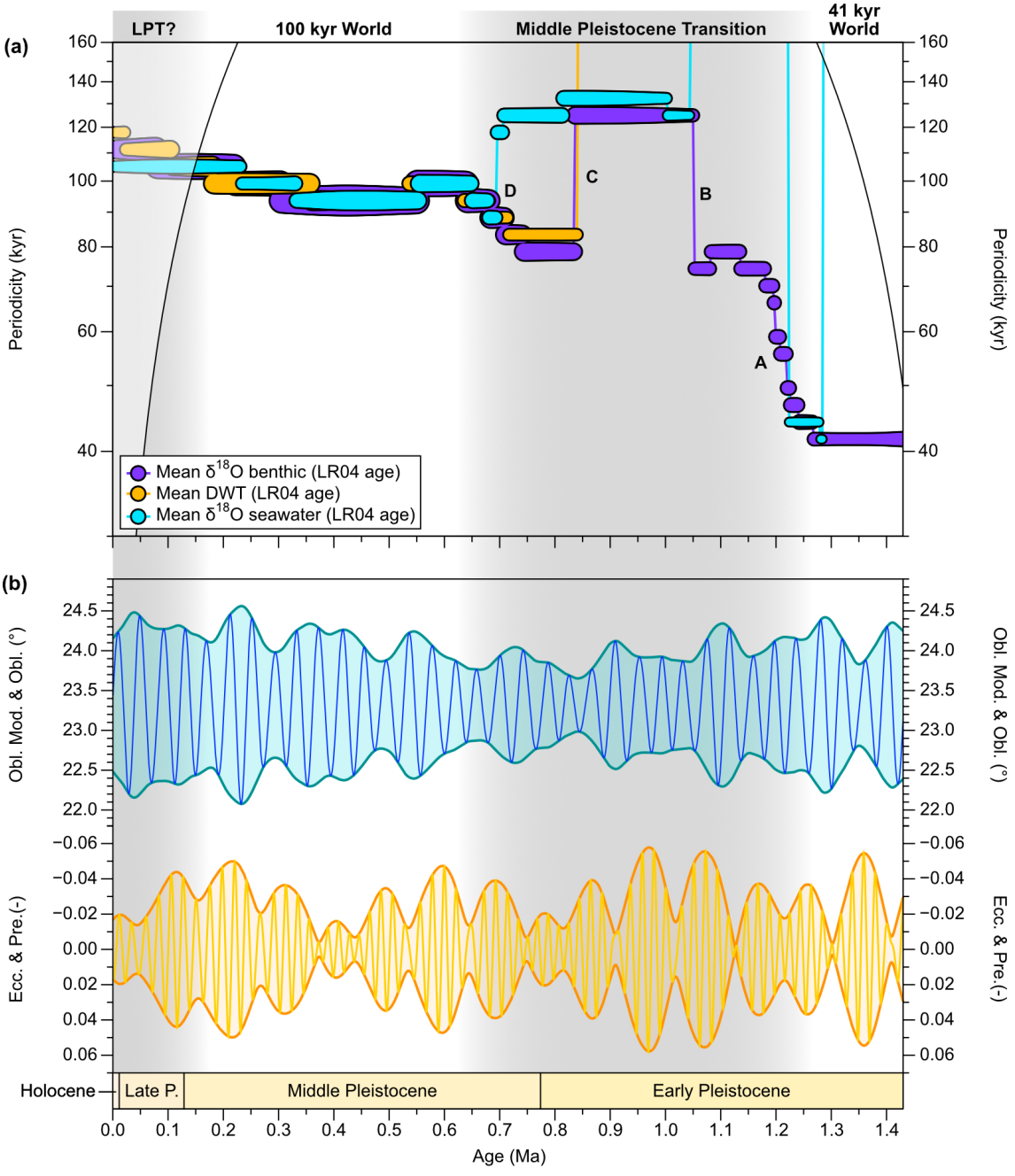


Figure 11: Spectral evolution of globally averaged proxy records. (a) SPR1s of global mean benthic $\delta^{18}O$ (see Supp. Figs. S102 to S106) compared to those of DWT and $\delta^{18}O_{seawater}$ (see Figs. 8 to 10 and Supp. Figs. S107 to S117). Note that switch point C in mean benthic $\delta^{18}O$ is much delayed compared to the Site U1385 benthic $\delta^{18}O$ record. Thickness of lines scales with spectral power and, for visual purposes only, with the ordering of the SPRs on top of one another. (b) As in Fig. 3c.

https://doi.org/10.5194/egusphere-2026-7022
Preprint. Discussion started: 20 November 2026
© Author(s) 2026. CC BY 4.0 License.

5. Postscript concerning Mitsui (2026)

While this study was under review among the co-authors, a preprint of Mitsui (2026) appeared online (https://eartharxiv.org/repository/view/12589/). The study independently reached several conclusions that are broadly consistent with our own observations and prompted a few revisions to the present manuscript. Specifically, we adopted the terminology of Spectral Power Ridges (SPRs) in place of Lines of Maximum Amplitude, expanded our analyses to include a broader range of benthic and planktic $\delta^{18}O$ stacks to evaluate the reproducibility of the observed spectral transitions, and clarified the distinction between frequency-locking and phase-locking. Although the two phenomena often occur together, potentially giving rise to nonlinear interactions (Liebrand and de Bakker, 2019), the CWT framework employed here is primarily suited to tracking the evolution of frequency-locking through time.

Despite these similarities, important methodological differences remain between the two studies. Mitsui (2026) employed the Weighted Wavelet Z-transform (WWZ) (Foster, 1996), whereas our analyses are based on the CWT applied to records that preserve their observed red-noise, or power-law, spectral structure. Power-law scaling is a fundamental characteristic of climate variability (Hasselmann, 1976) and has been documented across timescales including the millennial-to-orbital range (Huybers and Curry, 2006). Accounting for this background spectral structure is important when assessing the relative amplitudes of spectral peaks and attributing variance to specific periodicities.

The methodological differences between the WWZ and CWT approaches may contribute to several discrepancies between the results of Mitsui (2026) and those presented here, particularly in the trajectories and rankings of the dominant SPRs. Nevertheless, the broad agreement between the two studies regarding the evolution of the principal Pleistocene periodicities provides independent support for the existence of the major spectral transitions identified in this study. We have cited Mitsui (2026) throughout this manuscript.

6. Conclusions

This study provides a new perspective on the pacing of Pleistocene climate variability by re-examining the temporal evolution of spectral power through time in benthic and planktic $\delta^{18}O$, DWT, and $\delta^{18}O_{seawater}$ records. The results demonstrate that climate variability during the MPT was highly non-stationary. This transition is recast as an intermediate state in which multiple orbital-scale beats coexisted. Spectral power was mainly distributed between ~82 kyr (2 × 41 kyr) and ~123 kyr (3 × 41 kyr) obliquity-derived periodicities before merging into the 95–105 kyr pacing that characterises the 100 kyr World. This merger is documented in both DWT and $\delta^{18}O_{seawater}$, suggesting that it reflects a broader climate-system reorganization rather than merely the physical merger of ice sheets. During the 100 kyr World, climate variability recorded in benthic and planktic $\delta^{18}O$, DWT, and $\delta^{18}O_{seawater}$ records continued to track changes in eccentricity-band periodicities, reflecting the strongly nonlinear way the climate system responded to orbital forcing. The exceptional amplitude of the eccentricity band broadly around 0.4 Ma, including MIS 11, may reflect constructive interference between the 2 × 41 kyr obliquity-derived

https://doi.org/10.5194/egusphere-2026-7022
Preprint. Discussion started: 20 November 2026
© Author(s) 2026. CC BY 4.0 License.

and 90–105 kyr eccentricity-band periodicities, amplified by interactions between the climate and (marine) carbon cycles. Our results also raise the possibility that the latest Pleistocene represents a departure from the canonical 100 kyr World. More broadly, the SPR framework provides a new perspective on the pacemakers of the Pleistocene ice ages.

Code availability.

We used the CWT Matlab script of Grinsted et al. (2004) (https://github.com/grinsted/wavelet-coherence). Our video scripts are adapted from Christopher Lum's YouTube video "Creating Movies and Animations in Matlab" (https://www.youtube.com/watch?v=3I1_5M7Okqo&t=780s) and are made available through the online repository Zenodo (https://doi.org/10.5281/zenodo.20272114).

Data availability.

No new data was generated as part of this study. The astronomical solutions of Laskar et al. (2004) can be accessed here: https://ssp.imcce.fr/insola/earth/online/earth/online/index.php. The benthic and planktic $\delta^{18}O$ records from IODP Site U1385 of Hodell et al. (2023), augmented by Hodell et al. (2026), can be downloaded here: https://doi.pangaea.de/10.1594/PANGAEA.951401, and here: https://publications.iodp.org/proceedings/397/204/SUPP_MAT/TABLES/397-U1385TABLES.XLSX, respectively. The benthic and planktic $\delta^{18}O$ stacks of Huybers (2007) can be downloaded here: https://www.ncei.noaa.gov/pub/data/paleo/contributions_by_author/huybers2006/. The tuned and untuned LR04 stacks of Lisiecki and Raymo (2005) and Lisiecki (2010) can be downloaded here: https://lorraine-lisiecki.com/stack.html. Probstack and Probstack LR04 of Ahn et al. (2017) can be downloaded here: https://github.com/seonminahn/HMM-Stack. The five Bigstacks of Zhou et al. (2026) can be downloaded here: https://yz3062.github.io/htmls/BIGSTACK_bokeh.html. The global compilations of deep-water temperature and $\delta^{18}O_{seawater}$ of Thomas et al. (2026) can be downloaded here: https://doi.pangaea.de/10.1594/PANGAEA.980075.

Supplement.

The Supplementary Movies, Supplementary Figures and Matlab scripts used for making the movies are made available through the online repository Zenodo (https://doi.org/10.5281/zenodo.20272114).

Author contributions.

DL and DAH designed the study. DL did the statistical analyses and made the movies and figures. DL wrote the original draft and DAH and CSM contributed to the final manuscript.

https://doi.org/10.5194/egusphere-2026-7022
Preprint. Discussion started: 20 November 2026
© Author(s) 2026. CC BY 4.0 License.

Competing interests.

The authors declare no competing interests.

Disclaimer.

Publisher's note:

Acknowledgements.

We would like to thank Anouk de Bakker for the suggestion to compute difference spectra. Microsoft Copilot was used to improve the clarity and readability of the manuscript by streamlining the text and reducing repetition. The authors take full responsibility for the accuracy of the final manuscript.

Financial support.

The authors received no financial support for this study.

Review statement.

Included by Copernicus.

References.

Abe-Ouchi, A., Saito, F., Kawamura, K., Raymo, M. E., Okuno, J. i., Takahashi, K., and Blatter, H.: Insolation-driven 100,000-year glacial cycles and hysteresis of ice-sheet volume, Nature, 500, 190-193, https://doi.org/10.1038/nature12374, 2013.

Ahn, S., Khider, D., Lisiecki, L. E., and Lawrence, C. E.: A probabilistic Pliocene–Pleistocene stack of benthic δ18O using a profile hidden Markov model, Dynamics and Statistics of the Climate System, 2, https://doi.org/10.1093/climsys/dzx002, 2017.

Bajo, P., Drysdale, R. N., Woodhead, J. D., Hellstrom, J. C., Hodell, D., Ferretti, P., Voelker, A. H. L., Zanchetta, G., Rodrigues, T., Wolff, E., Tyler, J., Frisia, S., Spötl, C., and Fallick, A. E.: Persistent influence of obliquity on ice age terminations since the Middle Pleistocene transition, Science, 367, 1235-1239, https://doi.org/10.1126/science.aaw1114, 2020.

Barker, S., Starr, A., van der Lubbe, J., Doughty, A., Knorr, G., Conn, S., Lordsmith, S., Owen, L., Nederbragt, A., Hemming, S., Hall, I., Levay, L., Party†, I. E. S. S., Berke, M. A., Brentegani, L., Caley, T., Cartagena-Sierra, A.,

https://doi.org/10.5194/egusphere-2026-7022
Preprint. Discussion started: 20 November 2026
© Author(s) 2026. CC BY 4.0 License.

Charles, C. D., Coenen, J. J., Crespin, J. G., Franzese, A. M., Gruetzner, J., Han, X., Hines, S. K. V., Jimenez Espejo, F. J., Just, J., Koutsodendris, A., Kubota, K., Lathika, N., Norris, R. D., Periera dos Santos, T., Robinson, R., Rolison, J. M., Simon, M. H., Tangunan, D., Yamane, M., and Zhang, H.: Persistent influence of precession on northern ice sheet variability since the early Pleistocene, Science, 376, 961-967, https://doi.org/10.1126/science.abm4033, 2022.

Barker, S., Lisiecki, L. E., Knorr, G., Nuber, S., and Tzedakis, P. C.: Distinct roles for precession, obliquity, and eccentricity in Pleistocene 100-kyr glacial cycles, Science, 387, eadp3491, https://doi.org/10.1126/science.adp3491, 2025.

Bereiter, B., Eggleston, S., Schmitt, J., Nehrbass-Ahles, C., Stocker, T. F., Fischer, H., Kipfstuhl, S., and Chappellaz, J.: Revision of the EPICA Dome C CO_2 record from 800 to 600 kyr before present, Geophysical Research Letters, 42, 542-549, https://doi.org/10.1002/2014GL061957, 2015.

Berends, C. J., Köhler, P., Lourens, L. J., and van de Wal, R. S. W.: On the Cause of the Mid-Pleistocene Transition, Reviews of Geophysics, 59, e2020RG000727, https://doi.org/10.1029/2020RG000727, 2021.

Bintanja, R., and van de Wal, R. S. W.: North American ice-sheet dynamics and the onset of 100,000-year glacial cycles, Nature, 454, 869-872, https://doi.org/10.1038/nature07158, 2008.

Blackburn, T., Kodama, S., and Piccione, G.: Eccentricity Paces Late Pleistocene Glaciations, Geophysical Research Letters, 51, e2024GL108751, https://doi.org/10.1029/2024GL108751, 2024.

Cheng, H., Edwards, R. L., Broecker, W. S., Denton, G. H., Kong, X., Wang, Y., Zhang, R., and Wang, X.: Ice Age Terminations, Science, 326, 248-252, https://doi.org/10.1126/science.1177840, 2009.

Crowley, T. J., and Hyde, W. T.: Transient nature of late Pleistocene climate variability, Nature, 456, 226-230, https://doi.org/10.1038/nature07365, 2008.

Daubechies, I.: The wavelet transform, time-frequency localization and signal analysis, IEEE Transactions on Information Theory, 36, 961-1005, https://doi.org/10.1109/18.57199, 1990.

https://doi.org/10.5194/egusphere-2026-7022
Preprint. Discussion started: 20 November 2026
© Author(s) 2026. CC BY 4.0 License.

de Boer, B., Lourens, L. J., and van de Wal, R. S. W.: Persistent 400,000-year variability of Antarctic ice volume and the carbon cycle is revealed throughout the Plio-Pleistocene, Nature Communications, 5, 2999, https://doi.org/10.1038/ncomms3999, 2014.

Elderfield, H., Ferretti, P., Greaves, M., Crowhurst, S., McCave, I. N., Hodell, D., and Piotrowski, A. M.: Evolution of Ocean Temperature and Ice Volume Through the Mid-Pleistocene Climate Transition, Science, 337, 704-709, https://doi.org/10.1126/science.1221294, 2012.

Ford, H. L., and Raymo, M. E.: Regional and global signals in seawater $\delta^{18}O$ records across the mid-Pleistocene transition, Geology, 48, 113-117, https://doi.org/10.1130/g46546.1, 2019.

Foster, G.: Wavelets for period analysis of unevenly sampled time series, The astronomical journal, 112, 1709–1729, https://articles.adsabs.harvard.edu/pdf/1996AJ....112.1709F, 1996.

Ganopolski, A.: Toward generalized Milankovitch theory (GMT), Clim. Past, 20, 151-185, https://doi.org/10.5194/cp-20-151-2024, 2024.

Grinsted, A., Moore, J. C., and Jevrejeva, S.: Application of the cross wavelet transform and wavelet coherence to geophysical time series, Nonlin. Processes Geophys., 11, 561-566, https://doi.org/10.5194/npg-11-561-2004, 2004.

Hasselmann, K.: Stochastic climate models Part I. Theory, Tellus, 28, 473-485, https://doi.org/10.3402/tellusa.v28i6.11316, 1976.

Hays, J. D., Imbrie, J., and Shackleton, N. J.: Variations in the Earth's Orbit: Pacemaker of the Ice Ages, Science, 194, 1121-1132, https://doi.org/10.1126/science.194.4270.1121, 1976.

Herbert, T. D.: The Mid-Pleistocene Climate Transition, Annual Review of Earth and Planetary Sciences, 51, 389-418, https://doi.org/10.1146/annurev-earth-032320-104209, 2023.

https://doi.org/10.5194/egusphere-2026-7022
Preprint. Discussion started: 20 November 2026
© Author(s) 2026. CC BY 4.0 License.

Hodell, D., Lourens, L., Crowhurst, S., Konijnendijk, T., Tjallingii, R., Jiménez-Espejo, F., Skinner, L., Tzedakis, P. C., Abrantes, F., Acton, G. D., Alvarez Zarikian, C. A., Bahr, A., Balestra, B., Barranco, E. L., Carrara, G., Ducassou, E., Flood, R. D., Flores, J.-A., Furota, S., Grimalt, J., Grunert, P., Hernández-Molina, J., Kim, J. K., Krissek, L. A., Kuroda, J., Li, B., Lofi, J., Margari, V., Martrat, B., Miller, M. D., Nanayama, F., Nishida, N., Richter, C., Rodrigues, T., Rodríguez-Tovar, F. J., Roque, A. C. F., Sanchez Goñi, M. F., Sierro Sánchez, F. J., Singh, A. D., Sloss, C. R., Stow, D. A. V., Takashimizu, Y., Tzanova, A., Voelker, A., Xuan, C., and Williams, T.: A reference time scale for Site U1385 (Shackleton Site) on the SW Iberian Margin, Global and Planetary Change, 133, 49-64, https://doi.org/10.1016/j.gloplacha.2015.07.002, 2015.

Hodell, D. A., Channell, J. E. T., Curtis, J. H., Romero, O. E., and Röhl, U.: Onset of "Hudson Strait" Heinrich events in the eastern North Atlantic at the end of the middle Pleistocene transition (~640 ka)?, Paleoceanography, 23, https://doi.org/10.1029/2008PA001591, 2008.

Hodell, D. A., Crowhurst, S. J., Lourens, L., Margari, V., Nicolson, J., Rolfe, J. E., Skinner, L. C., Thomas, N. C., Tzedakis, P. C., Mleneck-Vautravers, M. J., and Wolff, E. W.: A 1.5-million-year record of orbital and millennial climate variability in the North Atlantic, Clim. Past, 19, 607-636, https://doi.org/10.5194/cp-19-607-2023, 2023.

Hodell, D. A., Crowhurst, S. J., Mleneck-Vautravers, M. J., Rolfe, J. E., Du, M., Herbert, T. D., Huang, H. H. M., Abrantes, F., Alvarez Zarikian, C. A., and the Expedition Scientists: Data report: composite section and chronology of IODP Sites 339-U1385 and 397-U1385 based on postcruise XRF analysis, Iberian Margin Paleoclimate, 397, https://publications.iodp.org/proceedings/397/ERR/CHAPTERS/397_204.PDF, 2026.

Huybers, P., and Curry, W.: Links between annual, Milankovitch and continuum temperature variability, Nature, 441, 329-332, https://doi.org/10.1038/nature04745, 2006.

Huybers, P.: Glacial variability over the last two million years: an extended depth-derived agemodel, continuous obliquity pacing, and the Pleistocene progression, Quaternary Science Reviews, 26, 37-55, https://doi.org/10.1016/j.quascirev.2006.07.013, 2007.

Huybers, P.: Pleistocene glacial variability as a chaotic response to obliquity forcing, Clim. Past, 5, 481-488, https://doi.org/10.5194/cp-5-481-2009, 2009.

https://doi.org/10.5194/egusphere-2026-7022
Preprint. Discussion started: 20 November 2026
© Author(s) 2026. CC BY 4.0 License.

King, T.: Quantifying nonlinearity and geometry in time series of climate, Quaternary Science Reviews, 15, 247-266, https://doi.org/10.1016/0277-3791(95)00060-7, 1996.

Kirtland Turner, S.: Pliocene switch in orbital-scale carbon cycle/climate dynamics, Paleoceanography, 29, 1256-1266, https://doi.org/10.1002/2014PA002651, 2014.

Laskar, J., Robutel, P., Joutel, F., Gastineau, M., Correia, A. C. M., and Levrard, B.: A long-term numerical solution for the insolation quantities of the Earth, A&A, 428, 261-285, https://doi.org/10.1051/0004-6361:20041335, 2004.

Lenoir, G., and Crucifix, M.: A general theory on frequency and time–frequency analysis of irregularly sampled time series based on projection methods – Part 1: Frequency analysis, Nonlin. Processes Geophys., 25, 145-173, https://doi.org/10.5194/npg-25-145-2018, 2018a.

Lenoir, G., and Crucifix, M.: A general theory on frequency and time–frequency analysis of irregularly sampled time series based on projection methods – Part 2: Extension to time–frequency analysis, Nonlin. Processes Geophys., 25, 175-200, https://doi.org/10.5194/npg-25-175-2018, 2018b.

Liautaud, P. R., Hodell, D. A., and Huybers, P. J.: Detection of significant climatic precession variability in early Pleistocene glacial cycles, Earth and Planetary Science Letters, 536, 116137, https://doi.org/10.1016/j.epsl.2020.116137, 2020.

Liebrand, D., de Bakker, A. T. M., Beddow, H. M., Wilson, P. A., Bohaty, S. M., Ruessink, G., Pälike, H., Batenburg, S. J., Hilgen, F. J., Hodell, D. A., Huck, C. E., Kroon, D., Raffi, I., Saes, M. J. M., van Dijk, A. E., and Lourens, L. J.: Evolution of the early Antarctic ice ages, Proceedings of the National Academy of Sciences, 114, 3867-3872, https://doi:10.1073/pnas.1615440114, 2017.

Liebrand, D., and de Bakker, A. T. M.: Bispectra of climate cycles show how ice ages are fuelled, Clim. Past, 15, 1959-1983, https://doi.org/10.5194/cp-15-1959-2019, 2019.

Lisiecki, L. E., and Raymo, M. E.: A Pliocene-Pleistocene stack of 57 globally distributed benthic $\delta^{18}O$ records, Paleoceanography, 20, https://doi.org/10.1029/2004PA001071, 2005.

https://doi.org/10.5194/egusphere-2026-7022
Preprint. Discussion started: 20 November 2026
© Author(s) 2026. CC BY 4.0 License.

Lisiecki, L. E.: Links between eccentricity forcing and the 100,000-year glacial cycle, Nature Geoscience, 3, 349-352, https://doi.org/10.1038/ngeo828, 2010.

Lourens, L. J., and Hilgen, F. J.: Long-periodic variations in the earth's obliquity and their relation to third-order eustatic cycles and late Neogene glaciations, Quaternary International, 40, 43-52, https://doi.org/10.1016/S1040-6182(96)00060-2, 1997.

Maslin, M. A., and Ridgwell, A. J.: Mid-Pleistocene revolution and the 'eccentricity myth', Early–Middle Pleistocene Transitions: The Land–Ocean Evidence, 247, 0, https://doi.org/10.1144/gsl.Sp.2005.247.01.02, 2005.

Mitsui, T.: Beyond the 100-kyr and 41-kyr dichotomy: ~76- and ~52-kyr signals and forbidden periodicities in Quaternary glacial cycles, Earth ArXiv (preprint), 1–52, https://doi.org/10.31223/X5419D, 2026.

Petrick, B., McClymont, E. L., Littler, K., Rosell-Melé, A., Clarkson, M. O., Maslin, M., Röhl, U., Shevenell, A. E., and Pancost, R. D.: Oceanographic and climatic evolution of the southeastern subtropical Atlantic over the last 3.5 Ma, Earth and Planetary Science Letters, 492, 12-21, https://doi.org/10.1016/j.epsl.2018.03.054, 2018.

Petrick, B., Martínez-García, A., Auer, G., Reuning, L., Auderset, A., Deik, H., Takayanagi, H., De Vleeschouwer, D., Iryu, Y., and Haug, G. H.: Glacial Indonesian Throughflow weakening across the Mid-Pleistocene Climatic Transition, Scientific Reports, 9, 16995, https://doi.org/10.1038/s41598-019-53382-0, 2019.

Pisias, N. G., and Moore, T. C.: The evolution of Pleistocene climate: A time series approach, Earth and Planetary Science Letters, 52, 450-458, https://doi.org/10.1016/0012-821X(81)90197-7, 1981.

Raffi, I., Wade, B. S., Pälike, H., Beu, A. G., Cooper, R., Crundwell, M. P., Krijgsman, W., Moore, T., Raine, I., Sardella, R., and Vernyhorova, Y. V.: Chapter 29 - The Neogene Period, Geologic Time Scale 2020, 1141-1215, https://doi.org/10.1016/B978-0-12-824360-2.00029-2, 2020.

Raymo, M. E., and Nisancioglu, K. H.: The 41 kyr world: Milankovitch's other unsolved mystery, Paleoceanography, 18, https://doi.org/10.1029/2002PA000791, 2003.

https://doi.org/10.5194/egusphere-2026-7022
Preprint. Discussion started: 20 November 2026
© Author(s) 2026. CC BY 4.0 License.

Raymo, M. E., Lisiecki, L. E., and Nisancioglu, K. H.: Plio-Pleistocene Ice Volume, Antarctic Climate, and the Global $\delta^{18}O$ Record, Science, 313, 492-495, https://doi.org/10.1126/science.1123296, 2006.

Ridgwell, A. J., Watson, A. J., and Raymo, M. E.: Is the spectral signature of the 100 kyr glacial cycle consistent with a Milankovitch origin?, Paleoceanography, 14, 437-440, https://doi.org/10.1029/1999PA900018, 1999.

Rodrigues, T., Alonso-García, M., Hodell, D. A., Rufino, M., Naughton, F., Grimalt, J. O., Voelker, A. H. L., and Abrantes, F.: A 1-Ma record of sea surface temperature and extreme cooling events in the North Atlantic: A perspective from the Iberian Margin, Quaternary Science Reviews, 172, 118-130, https://doi.org/10.1016/j.quascirev.2017.07.004, 2017.

Ruddiman, W. F., Raymo, M. E., Martinson, D. G., Clement, B. M., and Backman, J.: Pleistocene evolution: Northern hemisphere ice sheets and North Atlantic Ocean, Paleoceanography, 4, 353-412, https://doi.org/10.1029/PA004i004p00353, 1989.

Schulz, M., and Mudelsee, M.: REDFIT: estimating red-noise spectra directly from unevenly spaced paleoclimatic time series, Computers & Geosciences, 28, 421-426, https://doi.org/10.1016/S0098-3004(01)00044-9, 2002.

Shackleton, N. J., and Opdyke, N. D.: Oxygen-isotope and paleomagnetic stratigraphy of Pacific Core V28-239 Late Pliocene to Latest Pleistocene, Investigation of Late Quaternary paleoceanography and paleoclimatology, Memoir 145, 449–463, https://doi.org/10.1130/MEM145-p449, 1976.

Shackleton, N. J.: The 100,000-Year Ice-Age Cycle Identified and Found to Lag Temperature, Carbon Dioxide, and Orbital Eccentricity, Science, 289, 1897-1902, https://doi.org/10.1126/science.289.5486.1897, 2000.

Shackleton, N. J., Hall, M. A., and Vincent, E.: Phase relationships between millennial-scale events 64,000–24,000 years ago, Paleoceanography, 15, 565-569, https://doi.org/10.1029/2000PA000513, 2000.

Thomas, N. C., Ford, H. L., Greaves, M., and Hodell, D. A.: Increased abyssal ocean density stratification across the Middle Pleistocene Transition, Clim. Past, 2026, 1559–1584, https://doi.org/10.5194/cp-22-1559-2026, 2026.

https://doi.org/10.5194/egusphere-2026-7022
Preprint. Discussion started: 20 November 2026
© Author(s) 2026. CC BY 4.0 License.

Torrence, C., and Compo, G. P.: A Practical Guide to Wavelet Analysis, Bulletin of the American Meteorological Society, 79, 61-78, https://doi.org/10.1175/1520-0477(1998)079<0061:APGTWA>2.0.CO;2, 1998.

Tziperman, E., Raymo, M. E., Huybers, P., and Wunsch, C.: Consequences of pacing the Pleistocene 100 kyr ice ages by nonlinear phase locking to Milankovitch forcing, Paleoceanography, 21, https://doi.org/10.1029/2005PA001241, 2006.

Westerhold, T., Marwan, N., Drury, A. J., Liebrand, D., Agnini, C., Anagnostou, E., Barnet, J. S. K., Bohaty, S. M., De Vleeschouwer, D., Florindo, F., Frederichs, T., Hodell, D. A., Holbourn, A. E., Kroon, D., Lauretano, V., Littler, K., Lourens, L. J., Lyle, M., Pälike, H., Röhl, U., Tian, J., Wilkens, R. H., Wilson, P. A., and Zachos, J. C.: An astronomically dated record of Earth's climate and its predictability over the last 66 million years, Science, 369, 1383-1387, https://doi.org/10.1126/science.aba6853, 2020.

Wirths, C., Hermant, A., Stepanek, C., Stocker, T. F., and Sutter, J. C. R.: Sequence of abrupt transitions in Antarctic drainage basins before and during the Mid-Pleistocene Transition, Nature Communications, 16, 10391, https://doi.org/10.1038/s41467-025-65375-x, 2025.

Zhang, Z., Huang, Y., Ma, C., Yin, Q., Yang, H., Lee, E. Y., Cheng, H., Sames, B., Wagreich, M., Wang, T., Liu, Q., and Wang, C.: 100-kyr climate cycles caused by 2.4-Myr eccentricity-modulated carbon cycles, Nature Communications, 16, 8043, https://doi.org/10.1038/s41467-025-63403-4, 2025.

Zhou, Y., Lisiecki, L. E., Meyers, S. R., Lee, T., and Lawrence, C.: Global and regional Pleistocene benthic $\delta^{18}O$ stacks with a comparison of different age modeling strategies, Geochronology, 8, 85-107, https://doi.org/10.5194/gchron-8-85-2026, 2026.